

RESOURCE

Single-cell transcriptomic analysis of pea shoot development and cell-type-specific responses to boron deficiency

Xi Chen^{1,2,3} , Yanqi Ru¹ , Hirokazu Takahashi⁴ , Mikio Nakazono^{4,5} , Sergey Shabala^{1,2,3} , Steven M. Smith^{6,*}  and Min Yu^{1,5,*} 

¹Department of Horticulture, International Research Centre for Environmental Membrane Biology, Foshan University, Foshan 528000, China,

²Tasmanian Institute of Agriculture, University of Tasmania, Hobart, TAS 7001, Australia,

³School of Biological Science, University of Western Australia, Crawley, WA 6009, Australia,

⁴Graduate School of Bioagricultural Sciences, Nagoya University, Furo-cho, Chikusa, Nagoya 464-8601, Japan,

⁵School of Agriculture and Environment, University of Western Australia, Crawley, WA 6009, Australia, and

⁶Australian Research Council Centre of Excellence for Plant Success in Nature and Agriculture, School of Natural Sciences, University of Tasmania, Hobart, TAS 7001, Australia

Received 2 July 2023; revised 8 September 2023; accepted 20 September 2023; published online 5 October 2023.

*For correspondence (e-mail steven.smith@utas.edu.au; yumin@fusu.edu.cn).

SUMMARY

Understanding how nutrient stress impacts plant growth is fundamentally important to the development of approaches to improve crop production under nutrient limitation. Here we applied single-cell RNA sequencing to shoot apices of *Pisum sativum* grown under boron (B) deficiency. We identified up to 15 cell clusters based on the clustering of gene expression profiles and verified cell identity with cell-type-specific marker gene expression. Different cell types responded differently to B deficiency. Specifically, the expression of photosynthetic genes in mesophyll cells (MCs) was down-regulated by B deficiency, consistent with impaired photosynthetic rate. Furthermore, the down-regulation of stomatal development genes in guard cells, including homologs of *MUTE* and *TOO MANY MOUTHS*, correlated with a decrease in stomatal density under B deficiency. We also constructed the developmental trajectory of the shoot apical meristem (SAM) cells and a transcription factor interaction network. The developmental progression of SAM to MC was characterized by up-regulation of genes encoding histones and chromatin assembly and remodeling proteins including homologs of *FASCIATA1* (FAS1) and *SWITCH DEFECTIVE/SUCROSE NON-FERMENTABLE* (SWI/SNF) complex. However, B deficiency suppressed their expression, which helps to explain impaired SAM development under B deficiency. These results represent a major advance over bulk-tissue RNA-seq analysis in which cell-type-specific responses are lost and hence important physiological responses to B deficiency are missed. The reported findings reveal strategies by which plants adapt to B deficiency thus offering breeders a set of specific targets for genetic improvement. The reported approach and resources have potential applications well beyond *P. sativum* species and could be applied to various legumes to improve their adaptability to multiple nutrient or abiotic stresses.

Keywords: scRNA-seq, *Pisum sativum*, shoot development, boron deficiency, shoot apical meristem, guard cells.

INTRODUCTION

Boron (B) deficiency is a common problem causing reduced arable crop yields (Goldbach & Wimmer, 2007). Although B has been identified as an essential element for plants for 100 years (Warington, 1923), the fine print of its operation in plants at the molecular level remains to be

revealed, and any putative B receptors remain to be discovered. These challenges are mostly due to the fact that B is involved in numerous physiological and biochemical responses, making the separation of direct and indirect effects difficult. One of the direct pieces of evidence for the essentiality of B in plants is its role in maintaining the

structural stability of cell walls and membranes (O'Neill et al., 2001; Vioxeur & Fry, 2014). In plants, 90% of B is present in the cell wall, where it covalently cross-links two rhamnogalacturonan II (RG-II) monomers to form the dimeric RG-II-B, supporting cell wall structure and function (O'Neill et al., 1996). This role makes B essential for controlling plant architecture. However, whether different plant tissues exhibit different responses to B deficiency stress, whether different cell types have varying tolerances to B deficiency, and how aerial tissues adopt different strategies to adapt to B stress remains to be further investigated (Yang, Pan, et al., 2022).

In higher plants, the maturation of the shoot apical meristem (SAM) involves two main processes: maintaining the activity of the pluripotent stem cell population and the continuous differentiation of the meristem for the reiterated formation of lateral organs (Bowman & Eshed, 2000). The internal regulatory mechanisms of the SAM typically involve the activation of the CLAVATA3/EMBRYO SURROUNDING REGION (CLE) family by WUSCHEL (WUS) in the organizing center, maintaining stem cells through a signaling network. External regulation of the SAM includes the effects of environmental signals acting to influence the distribution of endogenous plant hormones, such as auxins and cytokinins, as well as modulation of signal perception to activate *WUS* expression (Bowman & Eshed, 2000; Zhang et al., 2017). Another homeodomain transcription factor (TF) isolated from a *Zea mays* mutant, KNOTTED1 (KN1) (*Arabidopsis thaliana* ortholog, SHOOTMERISTEM-LESS/STM), plays a role in preventing premature differentiation of meristem cells (Carles & Fletcher, 2003). Research has shown that meristem development is particularly sensitive to B deficiency (Poza-Viejo et al., 2018). The reduced-B-uptake mutant *tassel-less1* (*tls1*) in *Z. mays* exhibits defective SAM structure due to transcriptional repression of the meristem maintenance gene *KN1* and cell cycle genes (Matthes et al., 2022). However, how B deficiency affects the regulation of meristem development and the key TFs involved in this process have yet to be discovered.

Single-cell RNA-sequencing (scRNA-seq) achieves single-cell resolution for transcriptome sequencing of tissues. In addition to capturing even rare cell types, the spatiotemporal resolution of scRNA-seq helps us understand the relationships between cell types in space and time. By constructing developmental trajectories of cell types, we can reconstruct the differentiation process of a given tissue and the potential regulatory genes involved (Shaw et al., 2020). Currently, several studies have applied scRNA-seq or single-nucleus RNA-seq (snRNA-seq) to explore differences in cell types and developmental and differentiation trajectories in various plant species and tissues, including *A. thaliana* shoots and roots (Denyer et al., 2019; Zhang, Chen, & Wang, 2021), maize (*Z. mays*) shoots (Satterlee et al., 2020), rice (*Oryza sativa*) shoots and roots (Liu,

Liang, et al., 2021; Wang et al., 2021), poplar (*Populus*) stems and shoots (Chen et al., 2021; Conde et al., 2022), peanut (*Arachis hypogaea*) leaves (Liu, Hu, et al., 2021), tea (*Camellia sinensis*) leaves (Wang et al., 2022), *Medicago truncatula* root nodules (Ye et al., 2022), soybean (*Glycine max*) nodules (Liu et al., 2023) and wheat (*Triticum aestivum*) roots (Zhang et al., 2023). A few studies have also focused on the heterogeneous response of plant tissues under stress which include *Z. mays* roots in response to nitrate (Li et al., 2022), strawberry (*Fragaria vesca*) leaves in response to *Botrytis cinerea* infection (Bai et al., 2022), Chinese cabbage (*Brassica rapa*) leaves in response to heat stress (Sun, Feng, et al., 2022), rubber tree (*Hevea brasiliensis*) leaves in response to powdery mildew infection (Liang et al., 2023). However, the application of single-cell sequencing technology in the response of shoots to nutrient stress needs further investigation. scRNA-seq is rapidly advancing in the application of plant genomics research and is becoming an important tool for studying cell- and tissue-specific gene functions in plants.

Cell- and tissue-specific marker genes have been widely reported in well-annotated species such as *A. thaliana*, *O. sativa*, and *Z. mays*. They have been identified and validated by several techniques including reporter gene expression in transgenic plants, *in situ* hybridization to tissue sections, and laser capture microdissection (LCM) (Berkozitz et al., 2021; Bezrutczyk et al., 2021; Gala et al., 2021; Zhang, Chen, Liu, et al., 2021; Zhang, Chen, & Wang, 2021). However, reports of marker genes in legume plants, particularly in aerial tissues, are scarce. scRNA-seq enables the identification of new markers in other less-extensively studied species such as pea (*Pisum sativum*) by analyzing the transcriptomes of different cell types. LCM allows us to easily obtain different tissues within the shoot apex to verify the identification of new marker genes in such plants (Takahashi et al., 2010). With this powerful technology platform, it is now possible to study tissue-specific responses of agronomically important plants to biotic and abiotic stresses and uncover differential gene expression responses in specific cell types.

As the subject of Mendel's genetic research, *P. sativum* has become one of the more important subjects for plant genetics and developmental research due to its nitrogen-fixing ability, high nutritional value, and agricultural importance (Wong et al., 2008), with the world production of commercial *P. sativum* species estimated at 36.91 million tons (MT) in 2017 (Tassoni et al., 2020). The genomes of different *P. sativum* varieties have been sequenced, and the information is constantly being refined (Kreplak et al., 2019; Yang, Liu, et al., 2022). However, due to the large size of the *P. sativum* genome, the high proportion of repetitive sequences, and difficulties in applying functional genomics approaches, the annotation of *P. sativum* genes is lacking relative to soybean (*G. max*),

M. truncatula and *Lotus japonicus* (Smýkal et al., 2012). Therefore, the introduction of new omics technologies can help further develop *P. sativum* genomic resources and provide more information for genetic improvement and germplasm utilization.

In this study, we used a single-cell transcriptome approach to characterize the responses of shoot apical cells of *P. sativum* to B availability. The results reveal critical genes and regulatory factors related to shoot development in response to B deficiency and provide insights into strategies by which plants adapt to B deficiency thus offering breeders a set of specific targets for genetic improvement. The approach and resources could be applied to various legumes to improve their adaptability to multiple nutrient or abiotic stresses.

RESULTS

A single-cell atlas of *P. sativum* shoot apices

Pea (*P. sativum*) seeds were germinated in 0.5 mM CaCl₂ solution for 2 days, after which the seedlings were transferred to hydroponic culture in a 1/4 strength modified Hoagland nutrient solution with either 25 µM B (B25) or no B added (B0) for an additional 10 days. After 10 days of treatment, both the shoot and root of *P. sativum* showed B-deficient phenotypes (Figure S1a). Specifically, the fresh weight of both the shoot and root decreased (Figure S1b,d), while there was no significant change in dry weight (Figure S1c,e). The plant height was lower in B0 (Figure S1f). In both the entire shoot and root, compared to the B-supplied plants, B deficiency led to a threefold lower B content (Figure S1g,h). Subsequently, more than 50 shoot apices were collected for each treatment for scRNA-seq analysis. The apices were chopped with a razor blade and quickly transferred to 5 ml of cellulose and pectinase enzyme solution. After incubating for 1 h, cell number and viability were determined using light microscopy (Figure S2a) and staining with Trypan blue, respectively. More than 20 000 cells from each sample were labeled using the 10x Genomics scRNA-seq platform. Following the construction of cDNA libraries and Illumina high-throughput sequencing, gene expression levels were assessed by analyzing Unique Molecular Identifier (UMI) counts. The median number of genes detected per cell was 3416 (B0) and 2963 (B25), and the median UMI counts per cell were 10 567 (B0) and 8822 (B25). After filtering, a total of 14 493 high-quality cells were obtained from B25, with 25 390 genes mapped, while 9212 high-quality cells were obtained from B0, with 25 418 genes (Table S1). Seventy-seven percent of the genes identified by scRNA-seq were also detected in previous analysis of bulk RNA-seq data (Figure S2b) (Chen et al., 2022). Additionally, Pearson correlation analysis was performed on the 4000 genes showing the greatest fold change in response to B deficiency in bulk

RNA-seq and aggregated scRNA-seq data, revealing a correlation coefficient of 0.6 between the two platforms. Our results demonstrate a high degree of correlation between the genes induced by B deficiency across the two platforms.

The transcriptome data were then subjected to Principal Component Analysis (PCA) dimensionality reduction and clustering analysis, resulting in 15 distinct cell clusters, which were observed in both B25 and B0 (Figure S3a,b). To further elucidate the similarities and differences among cell clusters, we used the Uniform Manifold Approximation and Projection (UMAP) to visualize the cell clusters (Figure 1a). We used homologous genes in *P. sativum* of previously published marker genes from *A. thaliana* or *Z. mays* to identify each cell cluster (Figure 1b; Table S2). The average expression level of the marker gene used in each cell cluster is more than twice that of the same gene in other clusters. In mesophyll cells (MCs), CHLOROPHYLL A-B BINDING PROTEIN CP29.1 (Psat7g245920, PsLHCB4.1), CHLOROPHYLL A-B BINDING PROTEIN 215 (Psat2g004560, PsCAB215), PHOTOSYSTEM I CHLOROPHYLL A/B-BINDING PROTEIN 1 (Psat1g097880, PsLHCA1), and PHOTOSYSTEM I REACTION CENTER SUBUNIT III (Psat1g169240, PsPSAF) were highly expressed. In epidermal cells (ECs), HYDROXYSTEROID DEHYDROGENASE 1 (Psat7g037080, PsHSD1), LONG CHAIN ACYL-COA SYNTHETASE 1 (Psat6g160800, PsLACS1), LONG CHAIN ACYL-COA SYNTHETASE 2 (Psat7g206920, PsLACS2) and PALMITOYL-PROTEIN THIOESTERASE-DOLICHYL PYROPHOSPHATE PHOSPHATASE FUSION 1 (Psat0s4925g0080, PsPDF1) were highly expressed. In guard cells (GCs), EPIDERMAL PATTERNING FACTOR 1 (Psat5g271480, PsEPF1), TRANSCRIPTION FACTOR MUTE (Psat1g180920, PsMUTE), and TRANSCRIPTION FACTOR FAMA (Psat0s3505g0040, PsFAMA) were highly expressed. In vascular cells (VCs), HOMEOBOX-LEUCINE ZIPPER PROTEIN ATHB-8 (Psat5g020800, PsATHB-8), LEUCINE-RICH REPEAT RECEPTOR-LIKE PROTEIN KINASE TDR (Psat6g142440, PsTDR), COPPER TRANSPORT PROTEIN CCH (Psat6g093320, PsCCH), and PROTEIN SHORT-ROOT (Psat0s2268g0040, PsSHR) were highly expressed. GIBBERELLIN 2-BETA-DIOXYGENASE 1 (Psat1g189360, PsGA2OX1), HOMEOBOX PROTEIN KNOTTED-1-LIKE 3 (Psat6g028400, PsKNAT3), GLUTATHIONE S-TRANSFERASE U8 (Psat6g170320, PsGSTU8), and 9-CIS-EPOXYCAROTENOID DIOXYGENASE NCED1 (Psat1g001480, PsNCED1) were highly expressed and used as markers for SAM (Figure 1b; Table S2). Furthermore, significant expression of marker genes associated with cell proliferation was noted. HIGH MOBILITY GROUP B PROTEIN 6 (Psat7g026240, PsHMGB6), INFLORESCENCE MERISTEM RECEPTOR-LIKE KINASE 2 (Psat7g249120, PsIMK2), and UBIQUITIN-CONJUGATING ENZYME E2 20 (Psat7g179720, PsUBC20) serve as marker genes for proliferating cells (PCs), with notable expression in clusters 9 and 11 (Figure 1b; Table S2), indicating that these two cell clusters are engaged in cell division.

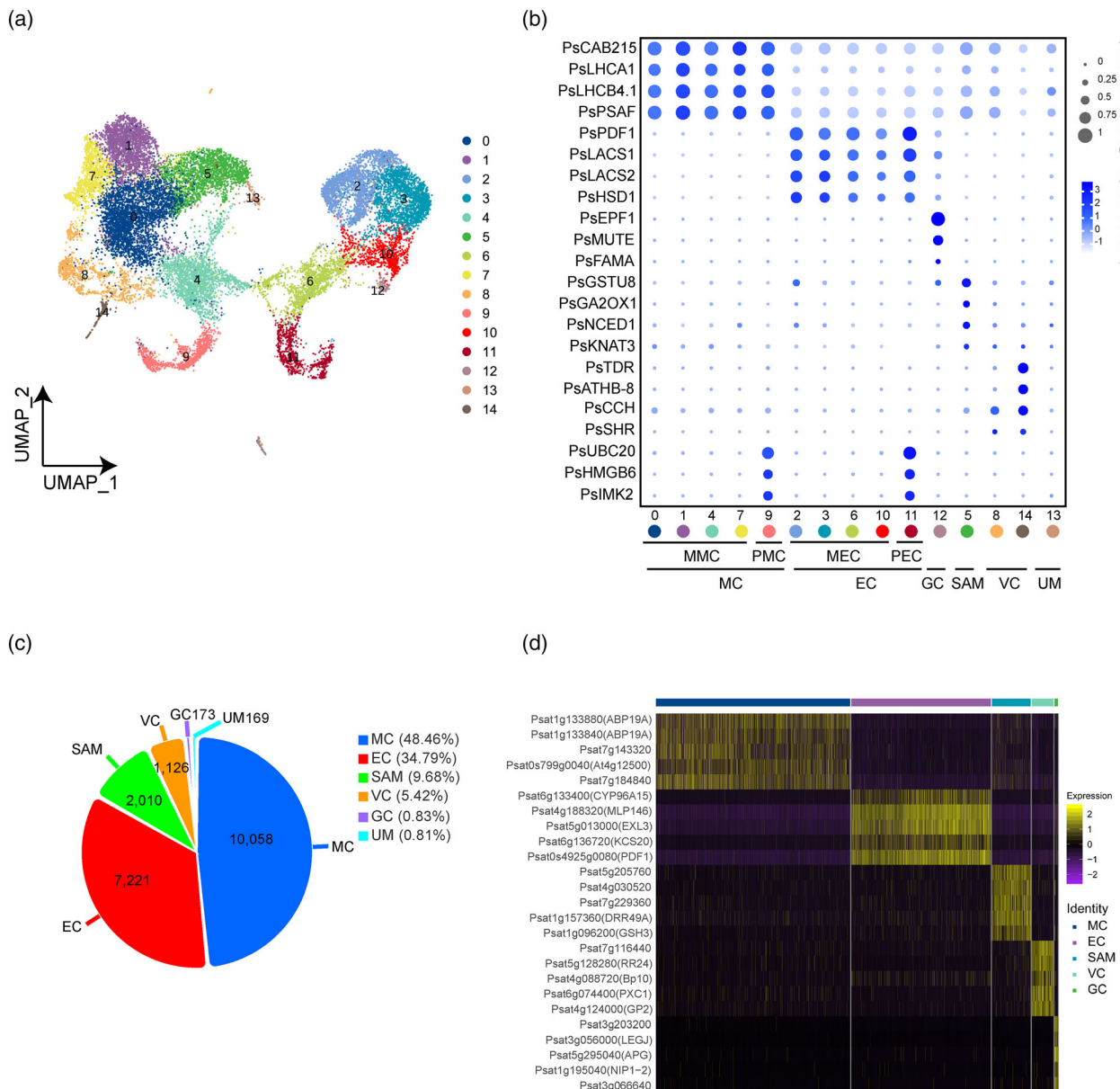


Figure 1. Classification of single-cell transcriptomes and cellular heterogeneity in pea (*Pisum sativum*) shoot apices.

(a) UMAP visualization of 15 cell clusters from 20 757 cells from B25 and B0. Each dot represents an individual cell.

(b) Expression pattern of cell-type-specific marker genes in each cell cluster. The dot size illustrates the percentage of cells expressing the gene, while the color intensity indicates the average expression level. Information on marker genes is given in Table S2.

(c) Pie chart showing cell types, the numbers of cells, and their proportions.

(d) Heatmap showing five characteristically up-regulated DEGs for all cells in each of five known cell types. Gene information is given in Table S3. Gene expression levels have been normalized by Z-score. DEG, differentially expressed gene; EC, epidermal cell; GC, guard cell; MC, mesophyll cell; MEC, mature epidermal cell; MMC, mature mesophyll cell; PEC, proliferating epidermal cell; PMC, proliferating mesophyll cell; SAM, shoot apical meristem; UM, unknown meristem; UMAP, Uniform Manifold Approximation and Projection; VC, vascular cell.

In summary, we identified clusters 0, 1, 4, 7, and 9 as MC populations (10 058 cells), clusters 2, 3, 6, 10, and 11 as EC populations (7221 cells), with 9 and 11 being PC populations of MC and EC, respectively. Cluster 12 was identified as GC population (173 cells), cluster 5 as SAM population (2010 cells), and clusters 8 and 14 as VC

population (1126 cells) (Figure 1c). Cluster 13 (169 cells) could not be successfully identified due to insufficient marker genes. However, it was classified as an unknown meristem (UM) population due to its transcript similarity to SAM cells (Figure 1a,c). We applied the Wilcoxon Rank Sum test in Seurat (R package) to analyze differentially

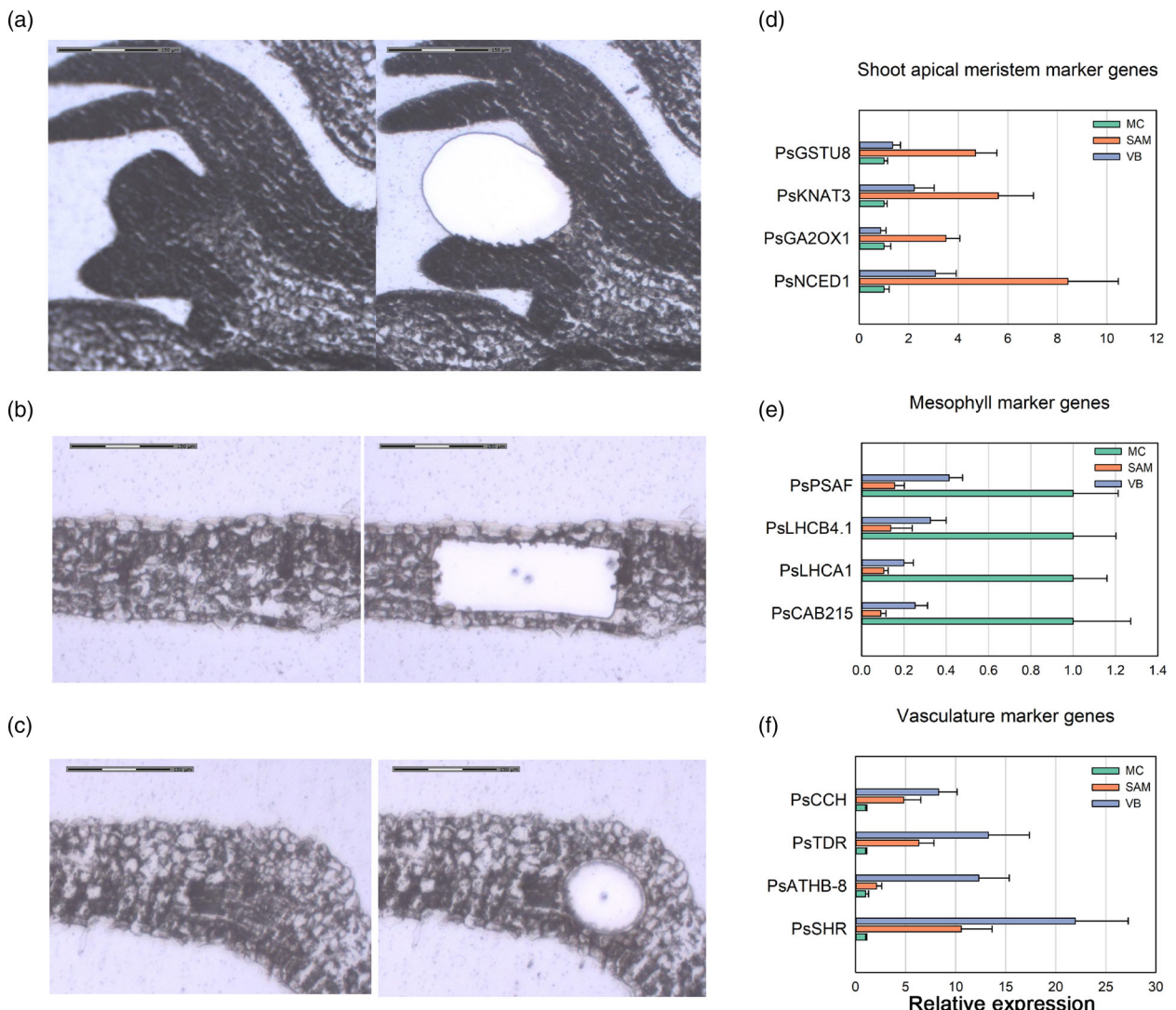


Figure 2. LCM of shoot apex and qRT-PCR showing the relative expression of marker genes in dissected tissues.

(a–c) Shoot apical meristem [SAM (a)], mesophyll cell [MC (b)], and vascular bundle [VB (c)] before and after LCM.

(d–f) Relative expression of marker genes for SAM (d), MC (e), and VB (f). Primer sequences are given in Table S12. *Actin* gene in *P. sativum* was used as a reference. Results were normalized relative to the expression in MC. Values represent mean \pm SD ($n = 3$). Scale bars (a–c): 150 μ m. LCM, laser capture microdissection.

expressed gene (DEG) expression among different cell types. We then screened for up-regulated genes in one type compared to others (these genes must be expressed in 25% of cells in the target or control type, with a $P \leq 0.01$, and a $\log_2\text{FC} \geq 0.36$) and showed the five most highly up-regulated DEGs in the five known cell types (Figure 1d; Table S3).

We used LCM to capture SAM, MC, and vascular bundle tissues from apices of *P. sativum* (Figure 2a–c), and the expression of the marker genes was validated by quantitative real-time PCR (qRT-PCR). We found that *PsKNAT3*, a gene that encodes a member of the KNOX (KNOTTED1-like homeobox) family that maintains stem cell stability, as

well as its downstream hormone signaling regulator *PsGA2OX1* and *PsNCED1*, regulated by CUC2 (CUP-SHAPED COTYLEDON 2) and BRC1 (BRANCHED1), were highly expressed in the SAM (Figure 2d). The *PsGSTU8* gene, a homolog of the *Z. mays* SAM marker, was validated to have a higher expression in *P. sativum* SAM (Figure 2d) (Satterlee et al., 2020). *PsPSAF*, *PsLHCB4.1*, *PsLHCA1*, and *PsCAB215*, functioning in photosynthesis, were highly expressed in MC (Figure 2e), while *PsCCH*, *PsSHR*, *PsATHB-8*, and *PsTDR* (*TDR/PXY*, *TDR/PHLOEM INTERCALATED WITH XYLEM*), which are involved in plant vascular development and differentiation, were highly expressed in the vascular bundle (Figure 2f). These results

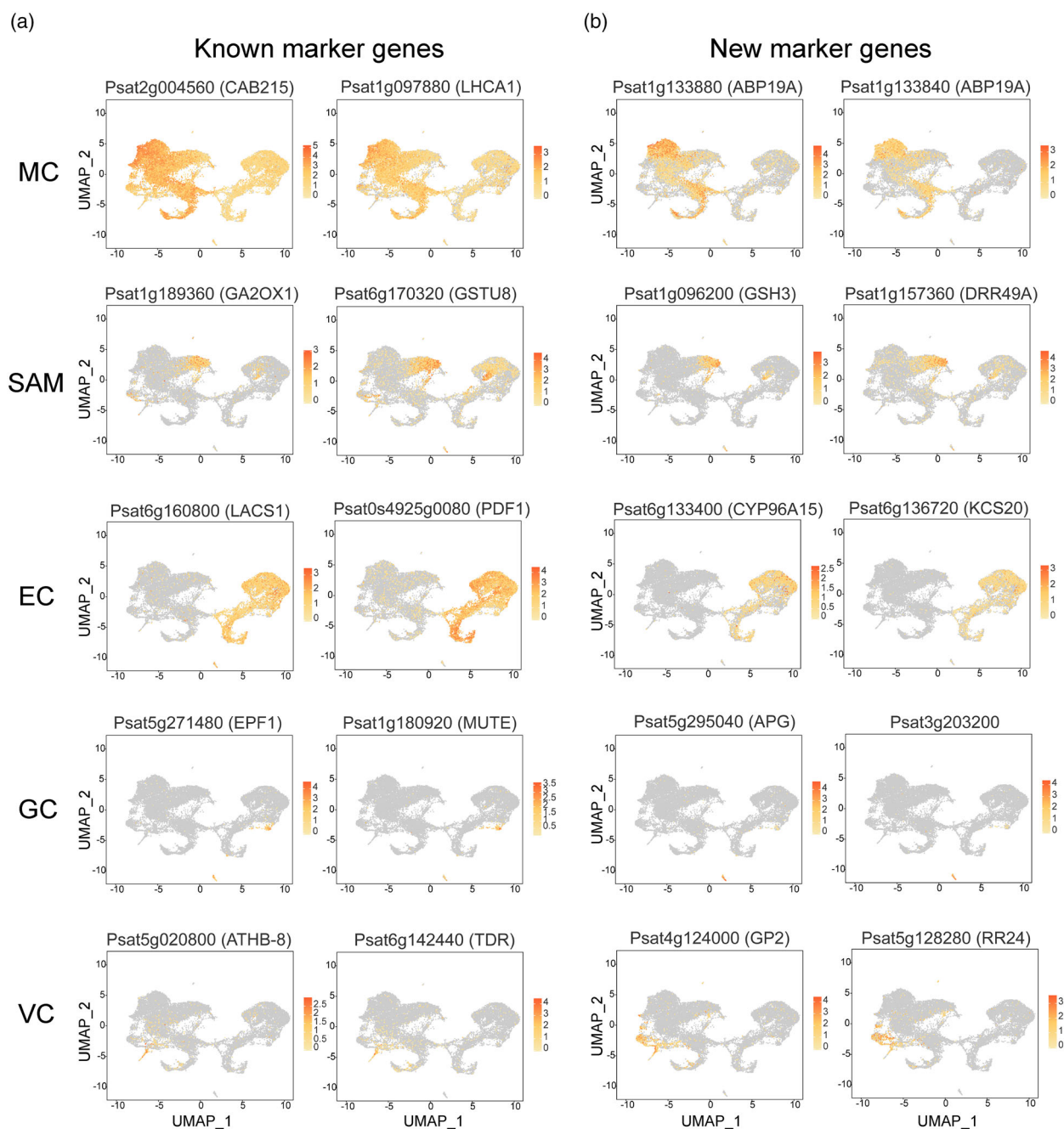


Figure 3. Expression of known marker genes (a) and new marker genes (b). UMAP plot illustrating the spatial distribution of expression of selected marker genes among different cell types. Color intensity reflects the level of gene expression. Gene information is given in Table S3. EC, epidermal cell; GC, guard cell; MC, mesophyll cell; SAM, shoot apical meristem; UMAP, Uniform Manifold Approximation and Projection; VC, vascular cell.

validate the reliability of our cell classification and demonstrate the accuracy of the new marker genes for cell-type-specific expression identified from this study (Figure 3). Our identification of cell types in *P. sativum* using scRNA-seq, as well as the validation of specific marker genes for these cell types, will be beneficial for recognizing different cell types in *P. sativum* and other legume plants in the future, as well as for further analyzing transcript level

differences between tissues. Functional genomics in legumes is difficult and relatively little research has been conducted so the identification of cell-type-specific marker genes will greatly facilitate research in *P. sativum* and other leguminous plants.

To further verify the accuracy of cell type identification and investigate the molecular characterization of each cell type, we conducted Gene Ontology (GO) and Kyoto

Encyclopedia of Genes and Genomes (KEGG) enrichment on the up-regulated cell-type-specific genes (Figures S4 and S5). The potential biological functions revealed through the enriched gene pathways help us to determine the accuracy of cell type identification. In MC, up-regulated genes were specifically enriched in photosynthesis, amino acids, and carbon metabolism, indicating that these genes are also related to primary functions such as energy metabolism. In SAM, up-regulated genes were specifically enriched in pathways such as plant hormone signal transduction and linolenic acid metabolism, revealing the key role of hormone signals in the shoot apex. In VC, genes involved in generating proton motive force via V-type H⁺-transporting ATPase were enriched, potentially providing energy for the uptake of inorganic and organic solutes. In EC, fatty acid metabolism pathways were enriched consistent with a crucial role in cuticle biosynthesis (Figures S4 and S5).

Responses to B deficiency in a cell-type-specific manner

By comparing the UMAP results of B25 and B0, we found that both include 15 cell clusters, indicating that the cell classification was not affected by B deficiency (Figure 4a,f, g). However, the transcript profiles of different cell types in response to B deficiency revealed some potentially important differences. The total number of captured cells in the B-deficient samples was lower, and the cell proportion also changed after B deficiency (Figure S3a). Boron deficiency resulted in a higher proportion of SAM and MC, while the proportion of EC and VC decreased (Table S4). Since the gene expression fluctuation in each cell is more sensitive in scRNA-seq compared to bulk RNA-seq, we used a lower threshold when screening for DEGs to avoid missing some potentially important DEGs. Genes with $|log_2FC| \geq 0.36$ and $P < 0.05$ were considered as DEGs. We identified the following numbers of DEGs in different cell types: 3402 in MC (2593 up, 809 down); 3046 in VC (1872 up, 1174 down); 2640 in EC (1993 up, 647 down); 2246 in GC (1380 up, 866 down); 2230 in SAM (1407 up, 823 down); 620 in UM (158 up, 462 down) (Figure 4b; Tables S5–S7).

Cell wall genes in different cell types

Since the most significant role of B is in maintaining cell wall structure (O'Neill et al., 2001), we analyzed the transcript levels of cell wall-related genes in different cell types under B deficiency. Among them, cellulose synthase genes (*CesA*) were up-regulated in all cell types, while some pectin synthesis-related genes (*GAUTs*, *GALACTURONOSYLTRANSFERASE*) were up-regulated in MC, VC, and SAM. In contrast, some pectin synthesis-related genes (*PMEs*) were down-regulated in SAM and GC. Cellulose degradation or modification genes (*XTHs*) were up-regulated in EC and GC. Polygalacturonase-related genes (*GPs*) were up-regulated in all cell types. However, cell wall loosening

EXPANSIN genes were down-regulated in all cell types (Table S8). Boron deficiency led to the remodeling of cell walls in different cell types of the shoot apex (Table S8, Chen et al., 2022). This deficiency also caused changes in pectin content and the pectic polysaccharide network, which in turn altered properties and compromised the stability of the cell wall (Fleischer et al., 1999). Boron deficiency could significantly influence cell wall integrity and function. The extent and nature of these effects, however, appear to be cell-type-specific, underscoring the complexity of B's role in cell wall maintenance and development.

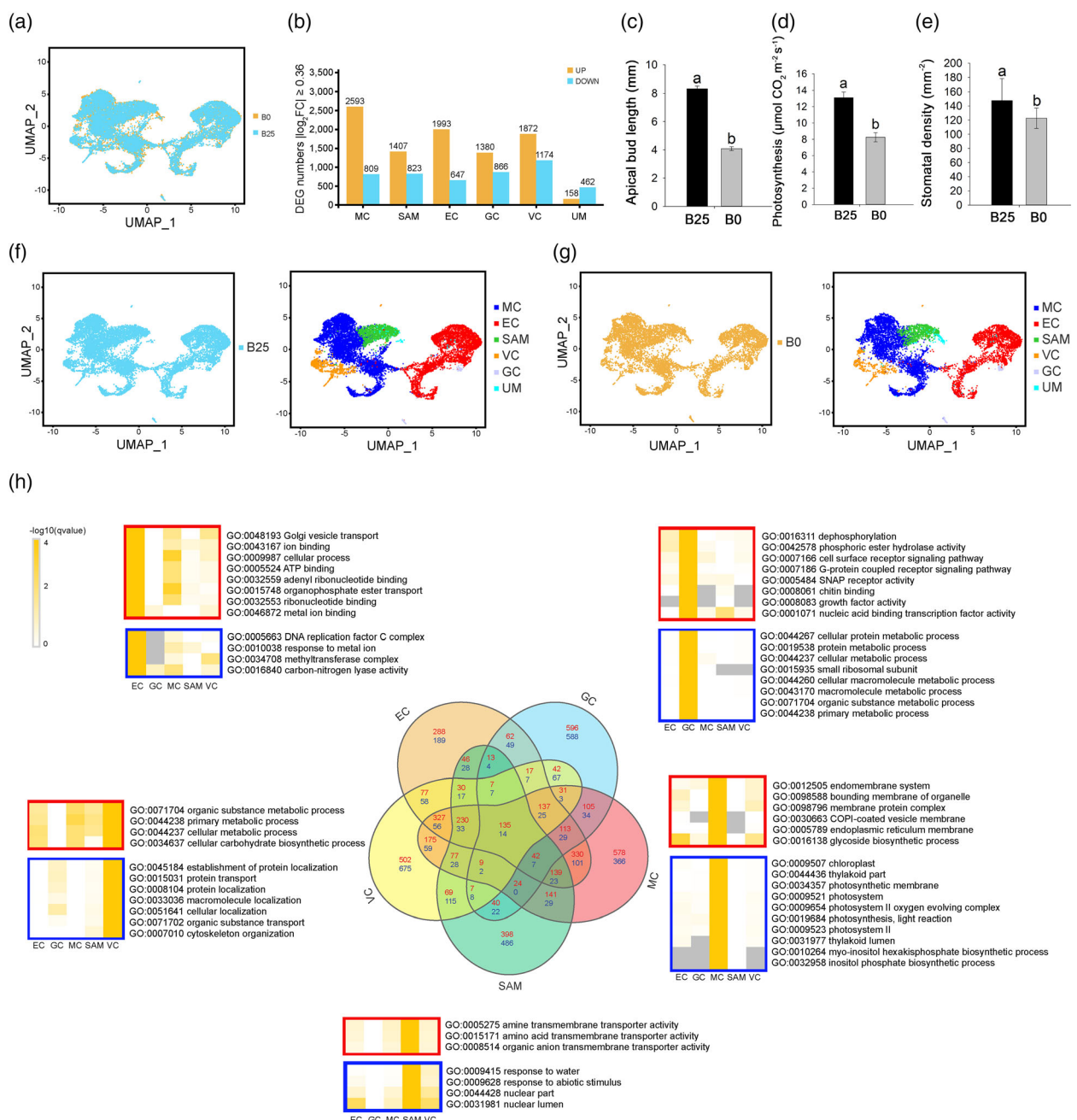
Analysis of DEGs in different cell types

We conducted GO enrichment analyses on these DEGs and showed specific enrichment in GO terms across different cell types (Figure 4h). Boron deficiency-induced up-regulation of genes related to Golgi vesicle transport, ion binding, and ATP binding functions in EC, but led to down-regulation of genes related to DNA replication and nucleotide excision repair. In EC, *PsPDF1*, which is related to epidermal-specific features and regulates epidermal development, was down-regulated by B deficiency (Table S5).

In VC, *SHORT ROOT (SHR)* genes (*Psat0s2268g0040*, *PsSHRa*; *Psat0s280g0040*, *PsSHRb*) regulating vascular tissue development were suppressed by B deficiency (Table S5), highlighting the importance of B in vasculature development. Boron transporter genes *PsBOR2* and *PsBOR6* were up-regulated in MC, SAM, EC, and VC under B deficiency (Table S9). This is consistent with previous results obtained from bulk RNA-seq (Chen et al., 2022). Plasma membrane intrinsic protein genes (*PIPs*) were also up-regulated in VC which indicates the regulation of water balance under B deficiency (Table S5).

In GC, B deficiency up-regulated genes are involved in dephosphorylation, cell surface receptor signaling pathways, and growth factor activity. The up-regulation of these genes may help activate the nutrient-stress adaptation mechanisms in GC, and enhance signal transduction to adapt to stress, while the enrichment results of down-regulated genes in GC indicate that protein synthesis and degradation processes, as well as amino acid synthesis pathways, are depressed in GC (Figure 4h; Tables S6 and S7). The *TRANSCRIPTION FACTOR SPEECHLESS* (*Psat6g038600*, *PsSPCH*), related to stomatal development, was up-regulated in GC, while *TOO MANY MOUTHS* (*Psat5g302680*, *PstTMM*) and *TRANSCRIPTION FACTOR MUTE* (*Psat1g180920*, *PsMUTE*) were down-regulated in GC (Table S5). Boron deficiency may suppress stomatal development during early aerial organ development by the inhibition of *MUTE* and *TMM*, which is consistent with decreased stomatal density under B deficiency (Figure 4e).

In MC, down-regulated genes were enriched in photosynthesis and chloroplast function-related pathways. The down-regulation of these genes due to B deficiency is

**Figure 4.** Cell-type-specific responses to B deficiency.

- (a) UMAP plot of *Pisum sativum* shoot apex cells of B25 (blue) treatment overlaid upon and B0 (orange) treatment (B25, 12 618 cells; B0, 8139 cells).
- (b) Numbers of DEGs (up, orange; down, blue) between B25 and B0 in six cell types. Detailed information of all the DEGs is given in Table S5.
- (c) Apical bud ($n = 12$) length difference between B25 and B0.
- (d) Photosynthesis rate ($n = 6$) difference between B25 and B0.
- (e) Stomatal density ($n = 24$) difference between B25 and B0. Values represent mean \pm SD. Lowercase letters indicate significant differences: Duncan's test ($P < 0.05$).
- (f, g) UMAP visualization of individual cells and distribution of identified cell clusters (color-coded) in B25 (F) and B0 (G) samples.
- (h) Venn diagram showing numbers of overlapping B-responsive DEGs (red, up in B0; blue, down in B0) between five known cell types (center) and Gene Ontology (GO) enrichment analysis (false discovery rate [FDR] ≤ 0.05) for B-responsive DEGs for each cell type (red boxes, up in B0; blue boxes, down in B0). DEG, differentially expressed gene; UMAP, Uniform Manifold Approximation and Projection.

consistent with the impaired photosynthesis efficiency of MC, which also explains the reduced plant growth rate and biomass accumulation. Photosynthesis-related genes,

including *PsPSAN*, *PsPSAL*, *PsPSAF* (photosystem I reaction center), *PsPSB28*, *PsPSBO*, *PsPSBY*, and *PsPNSL1* (photosystem II reaction center), were down-regulated. The

down-regulation of photosynthesis-related genes is consistent with the mechanism of reduced photosynthesis rate due to B deficiency from a tissue-specific perspective (Figure 4d) (Han et al., 2008).

Genes involved in meristem and MC development

WUSCHEL-related homeobox 8 (*Psat6g236200*, *PsWOX8*) was identified as a down-regulated DEG in both SAM and MC (Table S5). In addition, *LONELY GUY* (*LOG*) family members *Psat6g021440* (*PsLOG8*) and *Psat6g068040* (*PsLOG2*), which are involved in cytokinin metabolism, were down-regulated in MC and SAM, respectively (Table S5). These observations suggest that SAM activity and MC development might be impaired under B deficiency. After 10 days of B deficiency, the size of *P. sativum* apical buds was significantly reduced, consistent with such a conclusion (Figure 4c). In MC, *P. sativum* homologous genes *Psat6g028400* (*PsKNAT3*) and *Psat6s149g0040* (*PsKNAT4*) from the *KNOX* gene family, which induce leaf formation and development, were down-regulated (Table S5). Auxin-related genes were identified in all cell types and many were induced by B deficiency (Table S5). In these results, we observed that the process of SAM development leading to MC is coherent and highly significant. To further investigate the crucial regulatory factors involved in this process and the role of B, we conducted trajectory construction on specific cell types.

Cell differentiation trajectory of SAM to MC

During the development of the SAM, leaf primordia gradually expand and develop into mature leaves. Within this process, a subset of cells enters a proliferative phase, becoming what is referred to as proliferating mesophyll cells (PMCs). These PMCs not only express MC marker genes but also significantly express genes that have been identified as markers for proliferating cells (Figure 1b; Table S2). Eventually, as the leaf matures, the MCs that cease division transition into mature mesophyll cells (MMCs), at which point they become the primary sites of photosynthesis (Fleming, 2005). To assess the impact of B deficiency on this developmental process, pseudotime analysis was performed on SAM, UM, and MC, with SAM set as the starting point for pseudotime (Figure 5a,b). Both B25 and B0 samples were projected onto the three main branches of the pseudotime analysis, including four trajectory states, with cell differentiation increasing along the two trajectories as pseudotime progressed (Figure 5c; Figure S6d). SAM mainly clustered in state 1, PMC clustered in state 3, and MCs were identified in all the states (Figure S6a–e). Based on the differentiation pattern and the expression of photosynthesis-related genes, cell clusters in state 2 at the late stage of the pseudotime axis are proposed as MMCs (Figure 5c; Figure S6e). Boron deficiency significantly reduced the proportion of PMCs, indicating

that B deficiency affects the progress of differentiation of the tissue (Figure S6d,e). By analyzing the gene expression trends over pseudotime, we can decipher the impact of B deficiency on the different fates of SAM cells. Cells were allocated to three main states and two branches, based on the branching point that occurs when differentiating from state 1 to state 2 and state 3 (Figure S6a,c,e). The gene expression changes were categorized according to the trends over pseudotime and on different branches. Based on the similarity of expression trends, five gene clusters were obtained, with clusters 1 and 2 showing branch specificity (Figure 5d; Figure S6f). Cluster 1 genes show an up-regulated expression on the MMC branch as pseudotime progresses, while no significant changes are observed in PMC. Genes in cluster 1 have functions mainly related to DNA packaging, chromatin assembly, nucleosome assembly, and protein-DNA complex assembly pathways (Figure 5d; Table S10). This result indicates that chromatin structural changes mediated by histones play an important role in gene expression during SAM differentiation and development (Figure 6a–c). Additionally, the 6 histone-related DEGs showing the greatest fold difference over pseudotime change are displayed, revealing that these histone genes are highly expressed in the late stage of MC development (Figure 6b).

Boron deficiency was also found to suppress the expression of 83 histone genes (Figure 6d; Table S10), suggesting that B deficiency could induce chromatin structural changes by regulating histone gene expression, with these changes affecting the developmental process and fate of SAM cells. *PsFASCIATA1* (*PsFAS1*) was identified to be significantly downregulated only in SAM cells, and its expression was highly correlated with the SAM development process (Figure 6e–g). Cluster 2 genes are significantly up-regulated in the PMC branch, with no noticeable differences in MMC. Genes in cluster 2 show functions predominantly related to ribosome structure and function, and peptide biosynthetic processes (Figure 5d; Table S10). Boron deficiency leads to the down-regulation of a large number of such ribosome-related genes (Table S5). Meristem cells have a high protein synthesis activity (Murray et al., 2012). This activity is potentially reduced under B deficiency, potentially impairing cell proliferation.

Thus, we propose that B can regulate molecular pathways determining cell proliferation and cell fate in meristems. This function could explain the necessity of B for meristem function, and in turn, provides a molecular explanation for the role of B nutrition in plant growth and development.

Construction of a TF interaction network

In order to investigate the potential TFs involved in SAM development and the effects of B deficiency on the TF regulatory network, we examined the highly expressed TF

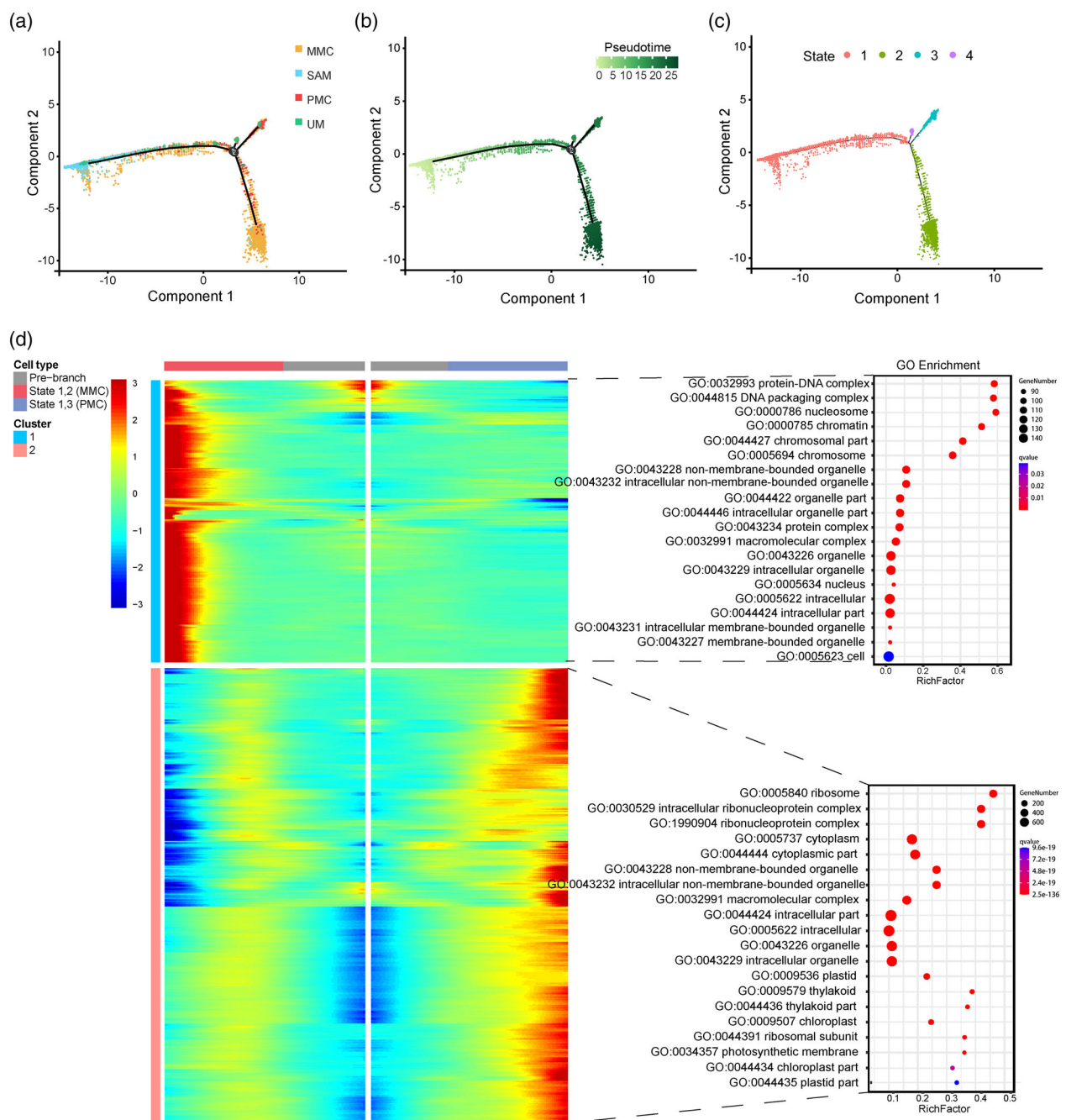


Figure 5. Differentiation trajectory from SAM to MC by pseudotime analysis.

(a–c) The distribution of cells along the pseudotime trajectory presented by cell types (a), pseudotime states (b), and branch states (c). (d) Branched heatmap showing DEGs with highly significant branch-specific expression patterns in pseudotime (q values less than 1×10^{-6}) and significantly enriched Gene Ontology (GO) terms ($q \leq 0.05$) showing the function of these genes. Detailed information of these genes is given in Table S10. The pre-branch point represents the beginning of pseudotime. Gene expression levels have been normalized by Z-score. Color bar for the heatmap indicates the relative expression level. The bubble color (red to violet) in the GO enrichment plot indicates the enrichment significance (q value) of the GO term, while the bubble size indicates DEG numbers enriched in each GO term. DEG, differentially expressed gene; MC, mesophyll cell; SAM, shoot apical meristem.

genes in different cell types and the effects of B deficiency on their expression. The greatest number of TF genes was identified in SAM (Figure 7a). However, B deficiency induced the expression of most TF genes in MC. Among

these, a large number of WRKY-family TF genes were significantly induced by B deficiency, including the previously reported B-responsive WRKY6 (Table S11) (Kasajima et al., 2010). In addition, we identified the up-regulation of

genes encoding TIFY family members, core components of the jasmonic acid signaling pathway, and the NAC family involved in plant growth and development. Some genes encoding members of the ethylene-responsive AP2/ERF family and cytokinin signaling pathway ARR-B family were induced by B deficiency in all cell types, indicating the importance of these TF gene families in response to B deficiency (Table S11). By constructing a protein interaction network of *A. thaliana* homologous TFs affected by B deficiency using STRING (Szklarczyk et al., 2018), we found that *SWI3A* and *SWI3C* interact with most TFs suggesting that they could be core components of a B-responsive TF co-response network (Figure 7b). *SWI2A* and *SWI3C* proteins are components of the SWITCH DEFECTIVE/SUCROSE NON-FERMENTABLE (SWI/SNF) chromatin remodeling complex. The SWI/SNF complex regulates gene expression by altering chromatin structure (Bieluszewski et al., 2023). In SAM, these two TF genes not only respond to B deficiency signals but also play a central regulatory role by interacting with other TFs. In addition, *TCP3*, *MYC2*, and *ERF4* also play potentially important regulatory roles (Figure 7b). Our previous bulk RNA-seq study showed that some TFs likely coordinate hormone signaling pathways to influence the response of *P. sativum* shoot apices to B deficiency stress (Chen et al., 2022). The current results further reveal the cell- and tissue-specific responses of TFs to B deficiency (Figure 7c).

DISCUSSION

Application of scRNA-seq to investigate the role of B

Although scRNA-seq has been applied in several studies of plants, its application in nutrient stress is limited. This study revealed cell-type-specific genes in *P. sativum* shoot apices and information on the transcript levels of cell-type-specific responses to B deficiency. It not only provides additional insights for unraveling cell specificity in the *P. sativum* genome but also identifies potential regulatory factors associated with shoot development in response to B deficiency.

Identification of cell types and their new markers in *P. sativum* shoot apices

As one of the more widely-studied plants, *P. sativum* shares many similarities with other dicotyledonous plants in its shoot apex. However, compared to *A. thaliana* there is much less information available at the molecular level because genome annotation and functional analysis has been less advanced in *P. sativum*. Furthermore, the lack of cell-type-specific marker genes in legume plants makes cell annotation more challenging. Although scRNA-seq studies of *L. japonicus* root (Sun, Jiang, et al., 2022) and *A. hypogaea* leaf (Liu, Hu, et al., 2021) have been published previously, no scRNA-seq data has been reported for legume shoot apices. In this study, we identify the transcript

differences among different cell types in *P. sativum* shoot apices as well as validate cell-type-specific markers using the LCM technology. In addition to validating markers homologous to some previously reported, we also identified new markers for different cell types in *P. sativum*. For example, *AUXIN BINDING PROTEIN 19A* (*PsABP19A*, *Psat1g133880*, *Psat1g133840*) was identified as a new marker for MC. We know that auxin signaling has a regulatory role in the differentiation fate and cell cycle of *A. thaliana* MCs, and the reprogramming of differentiated MCs is regulated by different auxin signals (Sakamoto et al., 2022). This suggests that in *P. sativum*, this gene may be important for MC development-related signaling. *CYTOCHROME P450 96A15* (*PsCYP96A15*, *Psat6g133400*) and *3-KETOACYL-COA SYNTHASE 20* (*PsKCS20*, *Psat6g136720*) were identified as new markers for EC. *AtKCS20* is involved in the synthesis of the important precursor of very long-chain fatty acids for *A. thaliana* epidermal cuticular wax (Lee et al., 2009). *AtCYP96A15* (also known as *ALKANE HYDROXYLASE MAH1*) is specifically expressed in *A. thaliana* pavement cells, and it also plays an essential role in cuticular wax synthesis in ECs (Greer et al., 2007). In addition to *GSTU8*, which was identified as a SAM marker in *Z. mays* (Satterlee et al., 2020), we also identified another glutathione-related gene, *GLUTAMATE DEHYDROGENASE 3* (*Psat1g096200*, *PsGSH3*), which is significantly up-regulated in SAM. This further suggests that glutathione transferases not only maintain the size and redox balance of root meristems (Horváth et al., 2019) but may also have important regulatory roles in SAM function. Further analysis of gene expression profiles in specific cell types is now possible and will provide valuable knowledge about the characteristics of each cell type, such as metabolism, differentiation, and responses to stress.

Shoot apex cells exhibit varying responses to B deficiency

Boron has an indispensable role in the structure and function of plant cell walls and membranes. It regulates cell wall formation by cross-linking two rhamnogalacturonan II (RG-II) monomers to form RG-II-B (O'Neill et al., 2001). Moreover, B can affect plasma membrane integrity by forming GIPC-B-RG-II complexes through RG-II and the membrane's GIPCs (Voxeur & Fry, 2014). One clear phenotype of B deficiency is the inhibition of root elongation (Poza-Viejo et al., 2018). Previous studies have shown that B deficiency affects normal physiological activities in the shoot, including impaired photosynthesis in MC (Figure 4d) (Han et al., 2008), impeding nutrient absorption and transport by affecting the stability of vascular bundles (Pommerening et al., 2019), and restricting the development of root meristem (Matthes et al., 2022). However, observing the effects of B deficiency on different cell types in the shoot apex at the single-cell transcript level is a novel aspect of this study.

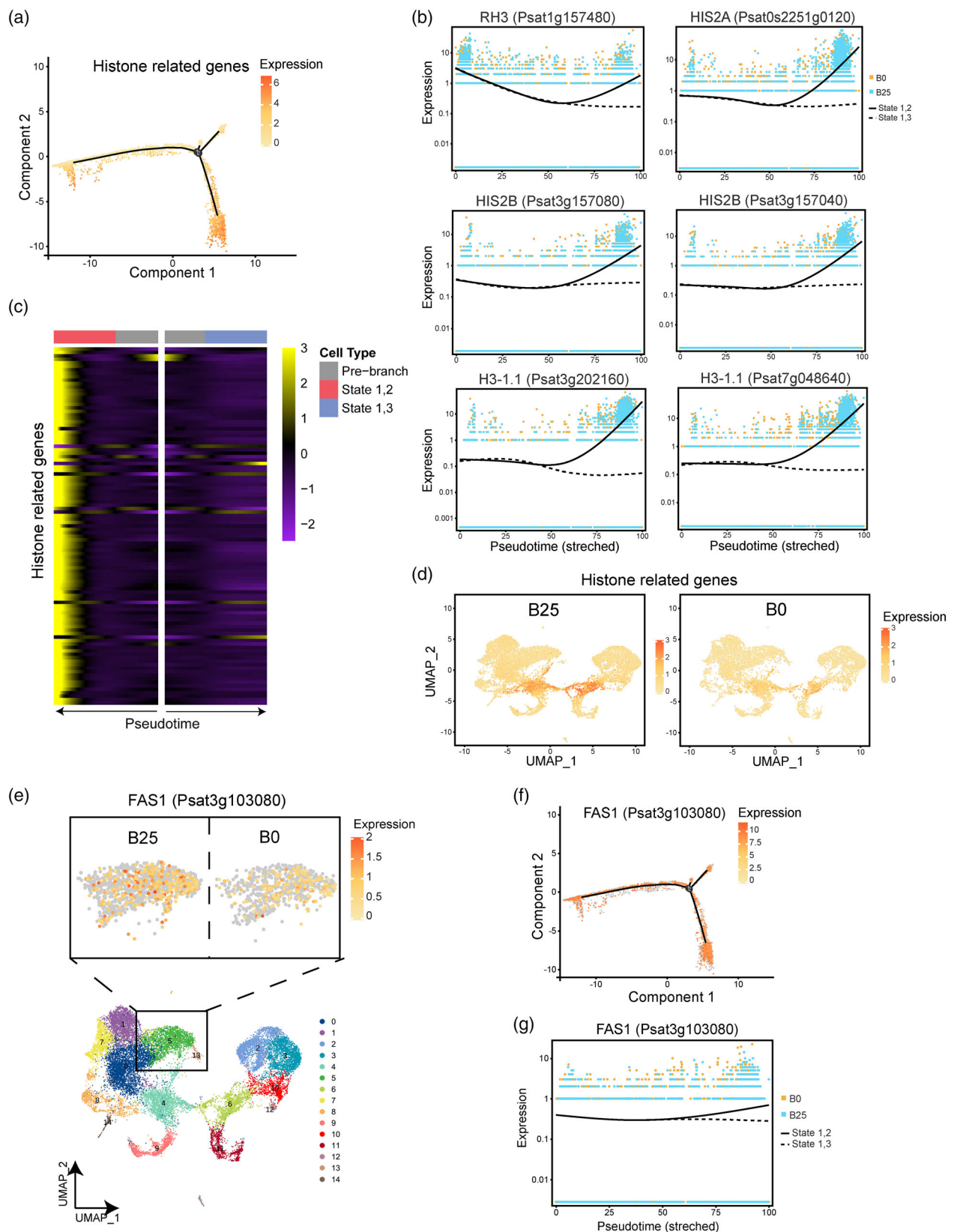


Figure 6. The expression patterns of histone-related genes and chromatin assembly factor subunit *FASCIATA1* in different cell fates and their responses to B deficiency.

- (a) Expression of histone-related genes along the pseudotime trajectory. Color intensity corresponds to expression level.
- (b) The expression trends of the six strongest histone-related DEGs before and after MC cell differentiation.
- (c) Heatmap showing all histone-related genes (DEGs) with significant expression trends in different branches. Information on these genes is given in Table S10.
- (d) UMAP plots showing the down-regulation of the histone-related genes under B deficiency. Color intensity corresponds to expression level.
- (e–g) The UMAP and pseudotime expression patterns of *PsFAS1* including down-regulation in SAM (cluster 5) under B deficiency (e), along the pseudotime trajectory (f) and different expression trends on the differentiation trajectory from SAM to MC (g). Solid lines represent expression from state 1 to state 2. Dashed lines represent expression from state 1 to state 3. Each dot represents an individual cell (blue dots represent cells of B25 while orange dots represent cells of B0). DEG, differentially expressed gene; MC, mesophyll cell; SAM, shoot apical meristem; UMAP, Uniform Manifold Approximation and Projection.

Boron deficiency does not affect the number of cell clusters predicted informatically, and all identified clusters appear in both B25 and B0 (Figure 4a,f,g). However, most genes respond to B deficiency in a cell-type-specific manner. Among them, the highest number of up-regulated DEGs was identified in MC, while the highest number of down-regulated DEGs was identified in VC (Figure 4b). Previous research has shown that in low-B-demanding rape-seed varieties, mesophyll and vascular growth can be maintained even under B starvation (Pommerenig et al., 2019). These findings emphasize the plasticity and adaptability of plant mesophyll and vascular cells in coping with B deficiency potentially by regulating gene expression in a cell-type-specific manner. Furthermore, when we applied a higher FC threshold to screen for DEGs, we found that GC, a less abundant cell type, had the most DEGs with FC greater than 2 (Figure S7). This suggests that although MC is more sensitive to moderate gene expression changes induced by B deficiency, GC may have a stronger response by specific genes. Due to the unique function and cell structure of GC, stomata are under rapid and dynamic control in response to abiotic stress (Hedrich & Shabala, 2018). The functions of strongly induced DEGs in GC under B deficiency are focused on cell surface receptor signaling, and abscisic acid (ABA)-related genes are also identified as significantly up-regulated in GC, indicating that GC responds to B deficiency through ABA signaling, leading to the activation of down-stream signals (Table S5). We also observed a decrease in stomatal density as a result of B deficiency (Figure 4e). These results not only point to the ABA-responsive mechanism of stomatal closure caused by B deficiency (Wimmer & Eichert, 2013) but also suggest the possibility of B deficiency affecting stomatal development at an early stage (Wei et al., 2022). A model was used to describe the cell-type-specific response mechanism of shoot apex under B deficiency (Figure 8).

Boron deficiency has a significant impact on the expression of cell wall biosynthesis and degradation-related genes, indicating that plants may maintain cell wall stability and structural integrity by adjusting the expression of cell wall-related genes under B deficiency (Chen et al., 2022). This response also shows some specificity in

different cell types. We found that cellulose synthase genes (*CesA*) were up-regulated in most of the cell types under B deficiency, which might reflect a strategy for plants to increase cellulose synthesis to strengthen cell wall structure in response to B deficiency. Polygalacturonase-related genes (*GPs*) were up-regulated in all cell types, suggesting that plants might increase pectin degradation to alleviate the negative effects of B deficiency on cell wall stability. We also observed that cellulose degradation enzyme genes encoding the XTH family (including both xyloglucan endotransglucosylase [XET] and xyloglucan endohydrolase [XEH] enzymes) were up-regulated in EC and GC, which could imply that plants might regulate cellulose degradation to alter cell wall elasticity and stability under B deficiency. Previous bulk RNA-seq results were consistent with B deficiency damaging the structure and function of the cell wall, triggering a series of compensatory mechanisms, leading to plants coping with such stress through biosynthesis and cell wall modification (Chen et al., 2022). The XTH family enzymes have different effects on the structure of the primary cell wall (Eklöf & Brumer, 2010). As the outermost cells, EC and GC have thicker cell walls and often exhibit rapid responses under stress (Javelle et al., 2011). The regulation of cell wall plasticity in response to B deficiency stress through the XTH family suggests that B deficiency impacts the cell wall integrity signaling in EC and GC (Humphrey et al., 2007).

The development of MCs from SAM

Since the application of scRNA-seq in plants, researchers have analyzed the single-cell transcriptome profiles of shoot apices in *A. thaliana* (Zhang, Chen, & Wang, 2021), *Z. mays* (Satterlee et al., 2020), and *populus* (Conde et al., 2022). These studies have demonstrated the high heterogeneity of shoot apical cells in different species, the continuous morphogenesis events in shoot development, and the identification of new regulatory factors in shoot development and physiology. One aim of the present study is to unravel how B deficiency affects apical bud development signals and to analyze the key regulatory factors involved in this process. To this end, we performed pseudotime analysis on SAM, MC, UM, and PMC, creating a differentiation trajectory for *P. sativum* shoot apices

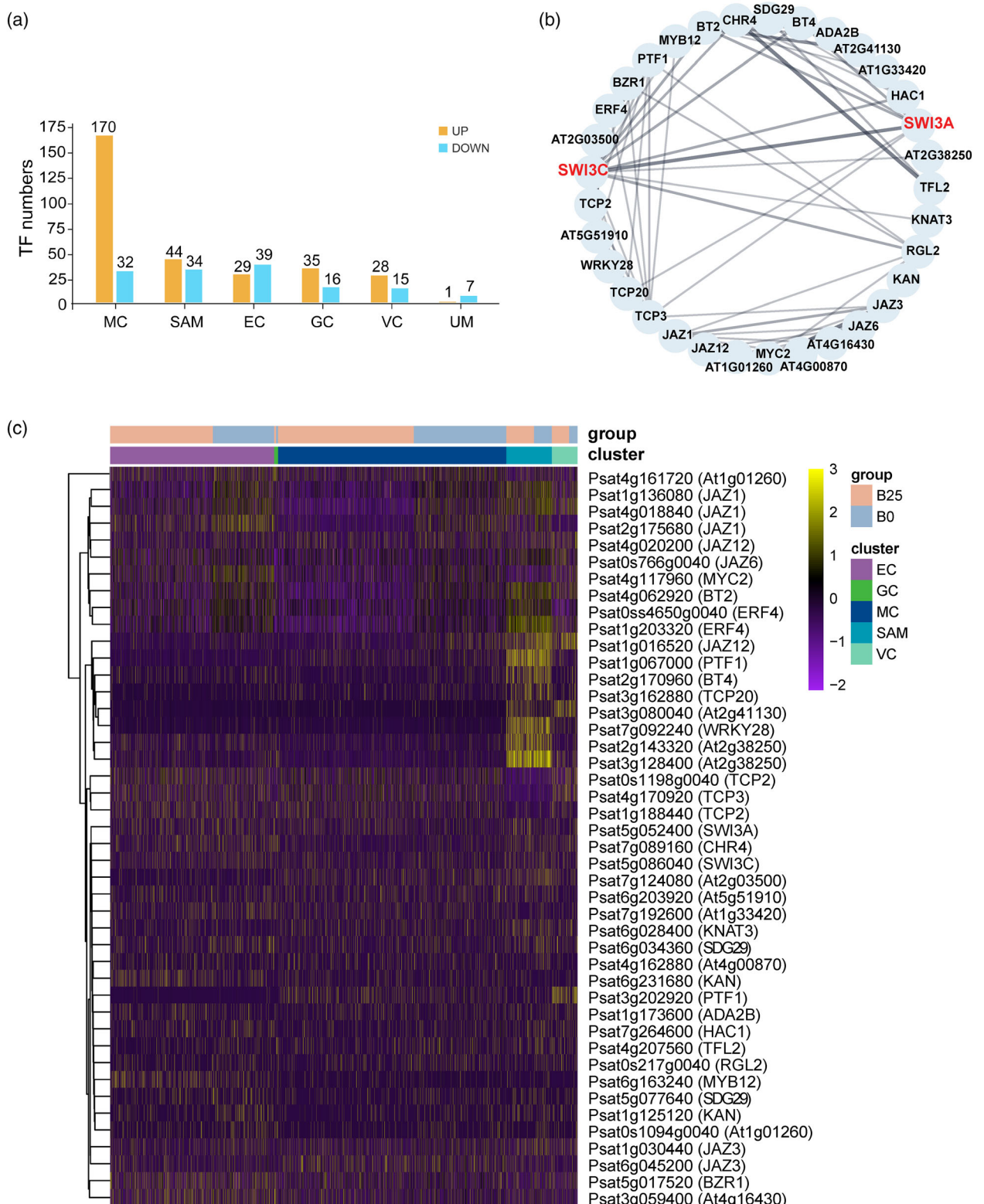


Figure 7. Transcription factor (TF) network analysis in cell-type-specific responses to B deficiency.

- (a) Numbers of differentially expressed TF genes in response to B deficiency. Genes upregulated (orange) or downregulated (blue) in B0 relative to B25. Information on these TF genes and their homologs in *A. thaliana* is given in Table S11.
- (b) Putative protein–protein interaction network of 33 differentially expressed TFs in response to B deficiency. String physical subnetwork was constructed using the homologs in *Arabidopsis thaliana*. SWI3A and SWI3C, shown in red, are the most connected proteins in this network.
- (c) Heatmap showing the cell-type-specific expression of 44 homologous *Pisum sativum* genes encoding these core TFs in response to B deficiency (up, yellow; down, purple).

(Figure 5a–c). Analyzing and annotating DEGs along different branches helps to identify key genes that determine or reflect cell fate. Moreover, the differences between samples can reveal the role of B in directing cell differentiation and determining the final cell fate. By clustering DEGs affecting the branching of developmental trajectories, we obtained five clusters (Figure S6f). We are particularly interested in genes in clusters 1 and 2, showing opposite expression patterns for specific genes in the two branches. Cluster 1 genes are significantly up-regulated in the MMC branch, while their expression levels are maintained in the PMC branch. Functional annotation analysis of the genes in this cluster reveals that their main functions are concentrated in DNA packaging, chromatin assembly, and nucleosome organization. We identified a large number of histone genes, including *H1*, *H2A*, *H2B*, and *H3*, that are significantly up-regulated in the branch determining the fate of MMCs (Figure 6c; Table S10). The organization and regulation of nucleosomes formed by DNA and histone octamers, as well as the regulation of higher-order chromatin condensation, play roles not only in transcription activation and repression but also in differentiation (Li et al., 2007). Chromatin is a dynamic structure that is constantly reshaped to activate or repress specific genes in response to cellular and environmental signals. Chromatin remodeling also plays a crucial role in regulating the *WUS* gene and maintaining the activity of meristematic tissues (Shen & Xu, 2009). By reconstructing cell differentiation trajectories and gene expression trends, we reveal the impact of chromatin structural changes regulated by histone genes on cell fate during *P. sativum* shoot apex differentiation and development.

Boron is required in meristem development regulated by histone-led chromatin remodeling

In meristem cells, the advantages of epigenetic regulation include the ability to store information, and provide stability, yet allow reversibility (Shen & Xu, 2009). As sessile organisms, plants rely heavily on chromatin-based mechanisms and subsequent transcriptional changes for their response mechanisms when faced with inescapable stresses (Probst & Scheid, 2015). For example, iron deficiency increases dissociation of Shk1 binding protein 1 (SKB1/AtPRMT5) from chromatin and reduces histone methylation levels, leading to enhanced transcription of *Bhlh*

genes and improved iron uptake in *A. thaliana* (Fan et al., 2014). The role of B in maintaining meristem development has been demonstrated in both shoots and roots (Abreu et al., 2014; Matthes et al., 2022). Based on our previous morphological analysis of shoot apices, B deficiency results in defects in SAM organization (Chen et al., 2022). Here, we propose a chromatin structure-mediated model in which B deficiency leads to changes in chromatin structure and accessibility, promoting the regulation of TFs, which in turn results in reduced meristem activity and impacts cell fate. In *A. thaliana*, CHROMATIN ASSEMBLY FACTOR-1 (CAF-1) consists of three subunits: FAS1, FAS2, and MULTICOPY SUPPRESSOR OF IRA1 (MSI1) (Shen & Xu, 2009). In *A. thaliana* *fas1* and *fas2* mutants, cell-specific expression of *WUS* is disrupted resulting in abnormal SAM development (Kaya et al., 2001). *PsFAS1* plays a regulatory role in determining cell differentiation fate, which is inhibited in SAM by B deficiency (Figure 6e–g). By elucidating the role of *PsFAS1* in regulating chromatin structure and identifying its response to B deficiency in SAM, our findings shed light on the mechanistic understanding of how B deficiency influences chromatin remodeling during shoot development. This chromatin structure-mediated model provides insights into the molecular processes underlying the effects of B deficiency on SAM organization and cell fate determination (Figure 8). Further research is warranted to unravel the precise molecular mechanisms and signaling pathways involved in this intricate regulatory network.

Potential role of SWI/SNF as a core TF in response to B deficiency

TF regulatory networks also play a crucial role in shoot apex development. Key TFs identified in bulk RNA-seq results, such as *PsWRKY40* and *PsERF4*, were also captured by scRNA-seq results (Figure 7b; Table S11). However, they were induced by B deficiency in different cell types. *PsWRKY40* was induced in MC, while *PsERF4* was induced in GC and VC, indicating that the expression of B deficiency-induced TFs is cell-type-specific. Members of the SWI/SNF complex, SWI3A and SWI3C, significantly responded to B deficiency in SAM and potentially act as core genes in the TF network, coordinating other TFs to regulate downstream signals. The SWI/SNF chromatin remodeling complex alters the contact between DNA and nucleosomes by utilizing ATP to make chromatin

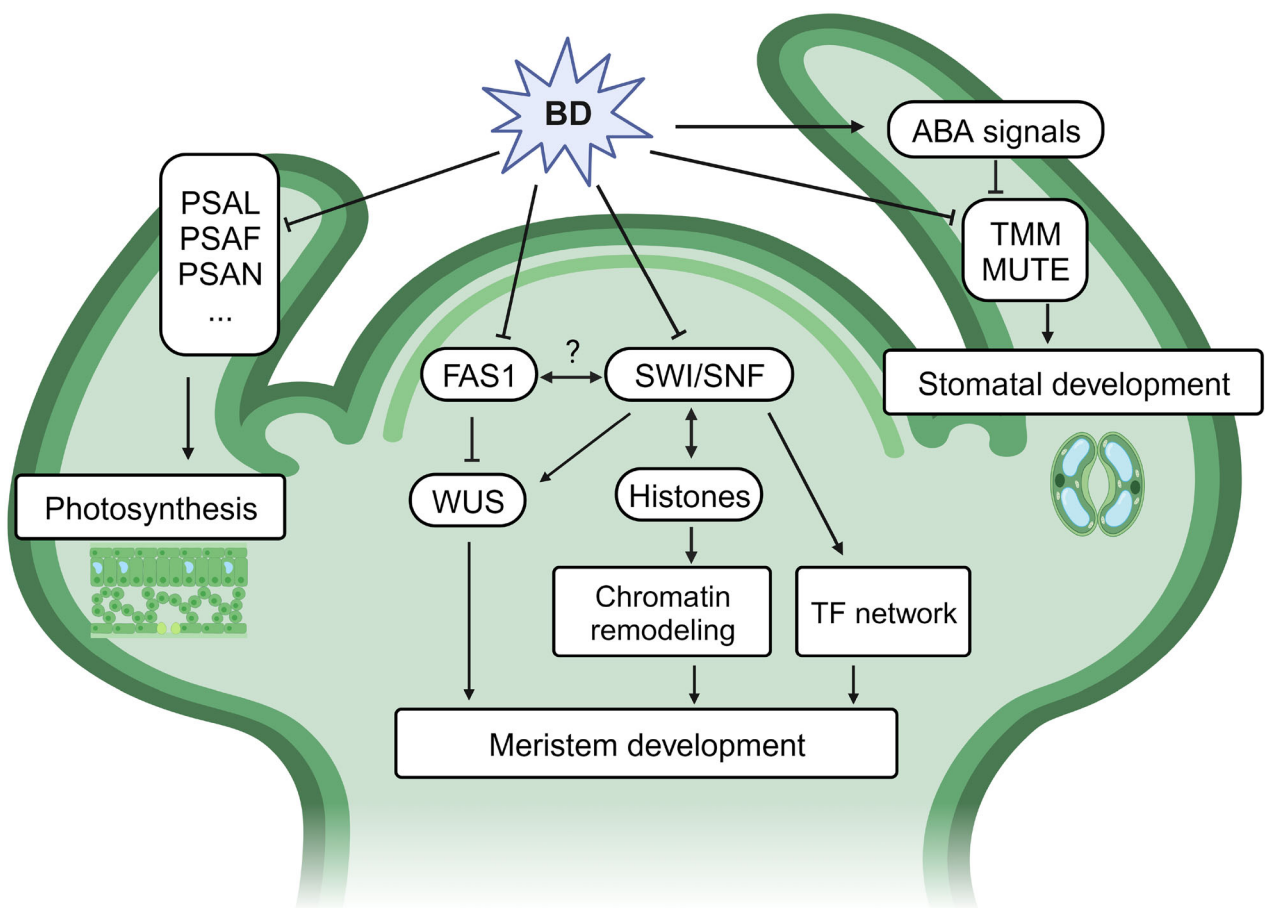


Figure 8. Schematic representation of the effect of B deficiency on shoot apex.

Boron deficiency potentially inhibits stomatal development by upregulating ABA signaling and suppressing genes related to stomatal development. Boron deficiency limits photosynthetic efficiency in MCs by repressing genes associated with photosynthesis. The impact of B deficiency on the development of SAM might be attributed to the suppression of signals involved in chromatin assembly and remodeling, primarily driven by FAS1 and SWI/SNF, which in turn inhibits differentiation of the meristem. Abbreviations: ABA, abscisic acid; BD, boron deficiency; FAS1, FASCIATA1; PSAF, PHOTOSYSTEM I REACTION CENTER SUBUNIT III; MC, mesophyll cell; PSAL, PHOTOSYSTEM I REACTION CENTER SUBUNIT XI; PSAN, PHOTOSYSTEM I REACTION CENTER SUBUNIT N; SAM, shoot apical meristem; SWI/SNF, SWITCH DEFECTIVE/SUCROSE NON-FERMENTABLE; TF, transcription factor; TMM, TOO MANY MOUTHS; WUS, WUSCHEL.

structures looser or tighter, thus affecting the accessibility of TFs and other regulatory proteins to specific genes (Bieluszewski et al., 2023). *WUS* expression in the OC region is activated by the SWI/SNF-type ATPase SYD (Shen & Xu, 2009). Our results suggest that SWI/SNF participates in the gene regulatory network under B deficiency.

CONCLUSION

This study demonstrates the power of the single-cell transcriptomics approach and reveals strategies by which plants adapt to conditions of B deficiency. Firstly, we show that responses of *P. sativum* shoot apices to B deficiency show highly pronounced heterogeneity, with distinct cell types exhibiting varying responses that correlated with their specific functions. The pronounced response observed in the GCs highlights their vital role in both withstanding external pressures and participating in signal transduction. Secondly, through pseudotime analysis, we

have constructed a developmental trajectory from SAM to MC and shown that chromatin structural changes, regulated by histones and FAS1, may serve as a crucial regulatory pathway governing the progression of SAM development. Collectively, these results led us to construct a schematic diagram that outlines the adaptive strategies employed by the shoot apex of *P. sativum* under B deficiency. By providing a precise transcriptome-level analysis, this study offers valuable insights for enhancing plant stress tolerance and for developing genotypes capable of coping with B stress not only in *P. sativum* but also in a broad range of legume species.

MATERIALS AND METHODS

Plant growth and treatment

Pea (*P. sativum*, cv. Caméor) seeds were treated with a 7.5% (w/v) sodium hypochlorite solution for 30 min, followed by soaking in a

0.5 mm CaCl₂ at 25°C in the dark for 8 h. Germination took place over 48 h in an aeroponic system containing 0.5 mm CaCl₂. Seedlings with roots 3–4 cm in length were then cultivated in a controlled environment room at 25°C in a one-fourth-strength modified Hoagland solution (pH 5.5), under a 16 h light (100 μmol photons m⁻² sec⁻¹) and 8 h dark cycle at 75% relative humidity. The B-free nutrient solution (B0) was prepared by removing B from water using an ion exchange resin (Amberlite IRA743 free base, Sigma-Aldrich, St. Louis, MO, USA) over 3 days. The B25 nutrient solution was prepared by adding 25 μM H₃BO₃ to the base solution. The nutrient solution was replaced every 4 days. These conditions have been previously optimized for the effects of B on the growth of *P. sativum* (Li et al., 2018; Yu et al., 2009).

Quantification of B content in shoot and root

To determine the B content, the Inductively Coupled Plasma-Optical Emission Spectrometry (ICP-OES, 700 series; Agilent Technologies, Palo Alto, CA, USA) was employed (Chen et al., 2022). Samples were prepared using six biological replicates, each composed of the entire shoot or root from 10 seedlings. These samples were initially oven-dried at 105°C for 30 min and subsequently dried at 65°C until they reached a stable weight. Once dried, the samples were ground with a ceramic mortar and pestle. The dry powder (30 mg per replicate) was added to a 10 ml solution of 1 M HCl. This mixture was then shaken vigorously for 2 h and subsequently filtered using a 0.22 μm Nylon 66 filter (Jinteng Experiment Equipment Co., Ltd, Tianjin, China). The ICP-OES technique was then utilized to assess the B concentration in the filtrate. A standard boric acid solution served as a reference for B quantification.

Protoplast preparation

After 10 days of hydroponic growth, the shoot apices were sampled for immediate protoplast isolation. Fifty shoot apices were cut into 1–2 mm strips and placed in a filtered enzyme solution containing 10 ml of 1.5% (w/v) cellulose R10, 1.5% (w/v) macerozyme R10, 0.5% (w/v) pectinase, 8% (w/v) mannitol (without Ca²⁺ and Mg²⁺), 0.02 M KCl, 0.01 M MES (Ph 5.7), 0.01 M CaCl₂, and 0.25% (w/v) BSA. The sample tube containing the enzyme solution and tissue was placed on an orbital shaker at 30°C with a shaking speed of 75 rpm in the dark for 1 h. The tissue was then washed twice with 8% (w/v) mannitol and filtered through a 40 μm cell strainer twice. A 5 μl protoplast suspension was mixed with 5 μl of 0.4% (w/v) trypan blue dye, and cell concentration and viability were measured using a hemocytometer and a light microscope. Finally, the protoplast suspension concentration was adjusted to 1000–2000 cells μl⁻¹ using an 8% (w/v) mannitol solution in preparation for loading onto the chromium controller of the 10x Genomics platform (10x Genomics, Pleasanton, CA, USA).

scRNA-seq library construction

Approximately 2 × 10⁴ isolated single cells and enzyme gel beads were packed into a single oil droplet for scRNA-seq library construction. The scRNA-seq libraries were constructed using the Chromium Single-Cell 3' GEM (Gel Beads-in-Emulsion) Library & Gel Bead Kit v3, following the user manual's instructions (10x Genomics). The Single-Cell 3' Library protocol generated standard Illumina paired-end constructs. The libraries were quality-checked using the High Sensitivity DNA Assay Kit (Agilent Technologies, Santa Clara, CA, USA). Finally, RNA quantification was performed using the ABI StepOnePlus Real-Time PCR System (Thermo Fisher Scientific, Waltham, MA, USA), followed by high-throughput

sequencing on the Illumina HiSeq2500. The 10X Genomics Cell Ranger software (10x Genomics, v3.1.0) was used for alignment and quantification. Cell Ranger employed the STAR (Spliced Transcripts Alignment to a Reference) aligner to map single-cell sequencing reads to the reference genome, *P. sativum* v1a (Kreplak et al., 2019). After filtering and correcting barcodes and UMIs, unique UMI counts and cell barcodes were used to generate gene-by-cell matrices for downstream analysis.

Data processing and cell clustering

First, the DoubletFinder was used to remove GEMs with doublets (McGinnis et al., 2019). The real doublets were distinguished from singlets by identifying real cells with high proportions of artificial neighbors in gene expression space. The low-quality cells were filtered out by setting cutoff values for the number of expressed genes per cell to greater than 500 and less than 8000. To visualize the data, dimension reduction and clustering analysis were performed on the raw count matrices using the Seurat (v3.1.1) package in R (v4.0.2). The data were reduced using PCA, and based on the classification results of cell subpopulations, UMAP was further employed to visualize the cell subpopulation classifications, resulting in 15 cell clusters. To identify these cell types, marker genes reported in *A. thaliana* and *Z. mays* were used, and *P. sativum* marker genes were obtained through orthologous gene comparison (Table S2). *A. thaliana* protein sequences were downloaded from TAIR (Garcia-Hernandez et al., 2002). In this way, six cell types were identified. Additionally, marker genes for each cell cluster were identified using the Wilcoxon Rank Sum test (with default parameters: likelihood ratio test) through the FindAll-Markers in Seurat. The filtering criteria for cell cluster-specific up-regulated genes were: genes expressed in more than 25% of cells in the target or control cluster, $P \leq 0.01$; and gene expression $\log_2 FC \geq 0.36$. When identifying DEGs within different cell types induced by B deficiency, we used a threshold of $|\log_2 FC| \geq 0.36$ and $P < 0.05$.

Gene enrichment analysis

All DEGs were assigned to GO terms in the GO database (<http://www.geneontology.org/>) and to pathway terms in the KEGG database (<http://www.genome.jp/kegg/>). A hypergeometric test was used to identify enriched GO and KEGG terms. GO and KEGG terms that were overrepresented and had a Benjamini-Hochberg adjusted P -value of less than 0.05 were included in subsequent analyses.

LCM and qRT-PCR

LCM was performed following existing methods (Takahashi et al., 2010). *P. sativum* shoot apices were embedded in paraffin (Paraplast Xtra; Fisher Scientific, Pittsburgh, PA, USA) using a previously reported microwave-based method (Takahashi et al., 2010). After slicing (10 μm thick) and transferring to microscope slides (PEN membrane glass slide; Thermo Fisher Scientific) and drying, MC, SAM, and vascular bundle cells were collected from different tissue sections using a Zeiss PALM MicroBeam Laser Microdissection System (Carl Zeiss, Jena, Germany). Each cell type had four replicates, and more than 300 sections were captured for each replicate. Subsequently, total RNA extraction was performed using a Pico-Pure™ RNA isolation kit (Thermo Fisher Scientific, Sunnyvale, CA, USA). The extracted total RNA was quantified using Quant-iT™ RiboGreen RNA reagent and kit (Invitrogen, Carlsbad, CA, USA). The quality of the total RNA extracted from target cells was evaluated using the RNA 6000 Pico kit on an Agilent 2100 Bioanalyzer (Agilent Technologies). RNA

integrity was determined based on the RNA Integrity Number (RIN) (Schroeder et al., 2006) and analyzed using 2100 Expert software (version B.02.02, Eukaryote Total RNA Pico Mode; Agilent Technologies). The RIN of each tissue was above 6, which meets the criteria for qRT-PCR analysis. The expression of marker genes was detected by qRT-PCR using the One-step TB Green Prime-ScriptTM RT-PCR kit II (Takara, Osaka, Japan). All genes were normalized against the level of an *actin* reference gene (Foo et al., 2005). Primer sequences are given in Table S12.

Pseudotime trajectory analysis

Pseudotime analysis was performed using Monocle (v3.0) to construct cell matrices and gene expression profiles, visualizing developmental trajectories while preserving the fundamental relationships among cell types in reduced dimensions (Trapnell et al., 2014). Monocle can utilize gene expression level signals in all cells and based on the pseudotime values of each cell, screen DEGs along the timeline to identify key genes related to developmental differentiation processes. The developmental trajectory was determined from SAM to MC and two distinct branches were identified. By clustering genes with similar expression trends, we identified DEGs that changed along the developmental trajectory. Their potential biological functions were further analyzed through GO and KEGG enrichment.

TF interaction network construction

To analyze core TFs, all expressed TFs in the samples were annotated using the plant TF database PlantTFDB (<http://planttfdb.cbi.pku.edu.cn>) (Guo et al., 2007). Differentially expressed TFs ($|\log_2\text{FC}| \geq 0.36$ and $P \leq 0.01$) were screened and B-responsive highly expressed TFs connected in the protein–protein interaction network using the STRING database. Finally, Pearson correlation coefficients (PCCs) were calculated between differentially expressed TFs and a co-expression network constructed using Cytoscape v3.7.2 (PCCs ≥ 0.6 , $P < 0.05$).

Data analysis and visualization

Data were analyzed using SPSS Statistics 20.0 (SPSS, Inc., Chicago, IL, USA). Duncan's least significant difference test was performed through analysis of variance (ANOVA) to determine the significance at $P < 0.05$. Visualization tools mainly used included Adobe Illustrator, R software, and OmicShare tools (<https://www.omicshare.com/tools>) (Gene Denovo Biotech. Co., Guangzhou, China).

AUTHOR CONTRIBUTIONS

XC, SMS, and MY conceptualized and supervised the research. XC and YR prepared the materials for scRNA-seq. XC performed data analysis. XC, HT, and MN performed and revised the LCM part. XC wrote the manuscript. XC, SS, SMS, and MY revised the manuscript.

ACKNOWLEDGEMENTS

This work was supported by the National Natural Science Foundation of China (Grant No. 32172672, 31672228, 31172038), Ministry of Science and Technology of China (CB02-07, WQ20174400441, 2018YFD0201203, G2021030008L, G2021030014L, DL20200230002), the Science and Technology Department of Guangdong Province (Grant No. 2018A050506085, 2015A040404048, 163-2018-XMZC-0001-05-0049, 2022B1212010015, 2017-1649), the Higher Education Department of Guangdong Province (Grant No. 2020KCXTD025),

MEXT KAKENHI (Grant No. JP20H05912) and the Australian Research Council (Grant No. CE200100015). Open access publishing facilitated by University of Tasmania, as part of the Wiley - University of Tasmania agreement via the Council of Australian University Librarians.

CONFLICT OF INTEREST

The authors declare that there is no conflict of interest.

DATE AVAILABILITY STATEMENT

Single-cell RNA-seq data have been deposited in the Sequence Read Archive (SRA) database at the National Center for Biotechnology Information (NCBI) under the accession number PRJNA983513.

SUPPORTING INFORMATION

Additional Supporting Information may be found in the online version of this article.

Figure S1. The effects of B deficiency on the growth of *P. sativum* at the time of sampling for scRNA-seq. (a) Images of whole plants grown in the presence (B25) or absence (B0) of B for 10 days. (b) Shoot fresh weight. (c) Shoot dry weight. (d) Root fresh weight. (e) Root dry weight. (f) Plant height. (g) Shoot B content. (h) Root B content. Values represent mean \pm SD ($n = 6$). Lowercase letters indicate significant differences: Duncan's test ($P < 0.05$).

Figure S2. Overview of scRNA-seq analysis. (a) Protoplast preparations for scRNA-seq. (b) Venn diagram showing numbers of unique and common genes detected in bulk RNA-seq and scRNA-seq in B0 and B25 samples.

Figure S3. Numbers of cells in each scRNA-seq cluster and correlation of each cluster. (a) Number of cells in each cluster in B0 and B25 samples. (b) Correlations between 15 cell clusters expressed as proportion of detected genes in common (greater than 0.5, red; less than 0.5, blue).

Figure S4. KEGG enrichment annotation of genes expressed specifically in the five known cell types. (a) SAM. (b) MC. (c) EC. (d) GC. (e) VC.

Figure S5. GO term enrichment annotation of genes expressed specifically in the five known cell types. (a) SAM. (b) MC. (c) EC. (d) GC. (e) VC.

Figure S6. Pseudotime trajectory from SAM to MC. (a–c) The distribution of cells along the pseudotime trajectory color-coded by cell type (a), pseudotime states, represented by intensity of green (b), and branch states, color-coded (c). MMC, mature mesophyll cells; SAM, shoot apical meristem cells; PMC, proliferating mesophyll cells; UM, unknown meristem. (d, e) Cell proportion of four states in B0 and B25 samples (d), and four different cell types (e). (f) Heatmap showing all gene clusters over the pseudotime trajectories.

Figure S7. Numbers of DEGs in response to B deficiency in six cell types. DEGs were identified as up (orange) or down (blue) in B0 relative to B25 with a fold-change of $|\log_2\text{FC}| \geq 1$.

Table S1. Single-cell sequencing results.

Table S2. Marker genes used for cluster annotation.

Table S3. Cluster-enriched genes information.

Table S4. Cell numbers change after boron deficiency (BD).

Table S5. Differentially expressed genes (DEGs) expression changes in different cell types.

Table S6. KEGG significant enrichment for DEGs from Table S5.

Table S7. GO significant terms for DEGs from Table S5.**Table S8.** Cell wall-related DEGs expression in different cell types.**Table S9.** Differentially expressed B transporters in different cell types.**Table S10.** Differentiation fate DEGs from pseudotime analysis (cluster1 and cluster2).**Table S11.** Transcription factor (TF) expression changes in different cell types.**Table S12.** Primer sequences used for qRT-PCR in laser capture microdissection (LCM).

REFERENCES

- Abreu, I., Poza, L., Bonilla, I. & Bolaños, L.** (2014) Boron deficiency results in early repression of a cytokinin receptor gene and abnormal cell differentiation in the apical root meristem of *Arabidopsis thaliana*. *Plant Physiology and Biochemistry*, **77**, 117–121. Available from: <https://doi.org/10.1016/j.jplphys.2014.02.008>
- Bai, Y., Liu, H., Lyu, H., Su, L., Xiong, J. & Cheng, Z.M.** (2022) Development of a single-cell atlas for woodland strawberry (*Fragaria vesca*) leaves during early *Botrytis cinerea* infection using single cell RNA-seq. *Horticulture Research*, **9**, uhab055. Available from: <https://doi.org/10.1093/hr/uhab055>
- Berkowitz, O., Xu, Y., Liew, L.C., Wang, Y., Zhu, Y., Hurgobin, B. et al.** (2021) RNA-seq analysis of laser microdissected *Arabidopsis thaliana* leaf epidermis, mesophyll and vasculature defines tissue-specific transcriptional responses to multiple stress treatments. *Plant Journal*, **107**, 938–955. Available from: <https://doi.org/10.1111/tpj.15314>
- Bezrutczyk, M., Zöllner, N.R., Kruse, C.P.S., Hartwig, T., Lautwein, T., Köhrer, K. et al.** (2021) Evidence for phloem loading via the abaxial bundle sheath cells in maize leaves. *Plant Cell*, **33**, 531–547. Available from: <https://doi.org/10.1093/plcell/kocab055>
- Bieluszewski, T., Prakash, S., Roulé, T. & Wagner, D.** (2023) The role and activity of SWI/SNF chromatin remodelers. *Annual Review of Plant Biology*, **74**, 139–163. Available from: <https://doi.org/10.1146/annurev-applant-102820-093218>
- Bowman, J.L. & Eshed, Y.** (2000) Formation and maintenance of the shoot apical meristem. *Trends in Plant Science*, **5**, 110–115. Available from: [https://doi.org/10.1016/S1360-1385\(00\)01569-7](https://doi.org/10.1016/S1360-1385(00)01569-7)
- Carles, C.C. & Fletcher, J.C.** (2003) Shoot apical meristem maintenance: the art of a dynamic balance. *Trends in Plant Science*, **8**, 394–401. Available from: [https://doi.org/10.1016/S1360-1385\(03\)00164-X](https://doi.org/10.1016/S1360-1385(03)00164-X)
- Chen, X., Humphreys, J.L., Ru, Y., He, Y., Wu, F., Mai, J. et al.** (2022) Jasmonate signaling and remodeling of cell wall metabolism induced by boron deficiency in pea shoots. *Environmental and Experimental Botany*, **201**, 104947. Available from: <https://doi.org/10.1016/j.envexpbot.2022.104947>
- Chen, Y., Tong, S., Jiang, Y., Ai, F., Feng, Y., Zhang, J. et al.** (2021) Transcriptional landscape of highly lignified poplar stems at single-cell resolution. *Genome Biology*, **22**, 319. Available from: <https://doi.org/10.1186/s13059-021-02537-2>
- Conde, D., Triozi, P.M., Pereira, W.J., Schmidt, H.W., Balmant, K.M., Knaack, S.A. et al.** (2022) Single-nuclei transcriptome analysis of the shoot apex vascular system differentiation in *Populus*. *Development*, **149**, dev200632. Available from: <https://doi.org/10.1242/dev.200632>
- Denyer, T., Ma, X., Klesen, S., Scacchi, E., Nieselt, K. & Timmermans, M.C.P.** (2019) Spatiotemporal developmental trajectories in the *Arabidopsis* root revealed using high-throughput single-cell RNA sequencing. *Developmental Cell*, **48**, 840–852. Available from: <https://doi.org/10.1016/j.devcel.2019.02.022>
- Eklöf, J.M. & Brumer, H.** (2010) The *XTH* gene family: an update on enzyme structure, function, and phylogeny in xyloglucan remodeling. *Plant Physiology*, **153**, 456–466. Available from: <https://doi.org/10.1104/pp.110.156844>
- Fan, H., Zhang, Z., Wang, N., Cui, Y., Sun, H., Liu, Y. et al.** (2014) SKB1/PRMT5-mediated histone H4R3 dimethylation of Ib subgroup *bHLH* genes negatively regulates iron homeostasis in *Arabidopsis thaliana*. *Plant Journal*, **77**, 209–221. Available from: <https://doi.org/10.1111/tpj.12380>
- Fleischer, A., O'Neill, M.A. & Ehwald, R.** (1999) The pore size of non-graminaceous plant cell walls is rapidly decreased by borate ester cross-linking of the pectic polysaccharide rhamnogalacturonan II. *Plant Physiology*, **121**, 829–838. Available from: <https://doi.org/10.1104/pp.121.3.829>
- Fleming, A.J.** (2005) The co-ordination of cell division, differentiation and morphogenesis in the shoot apical meristem: a perspective. *Journal of Experimental Botany*, **57**, 25–32. Available from: <https://doi.org/10.1093/jxb/eri268>
- Foo, E., Bullier, E., Goussot, M., Foucher, F., Rameau, C. & Beveridge, C.A.** (2005) The branching gene *RAMOSUS1* mediates interactions among two novel signals and auxin in pea. *Plant Cell*, **17**, 464–474. Available from: <https://doi.org/10.1105/tpc.104.026716>
- Gala, H.P., Lanctot, A., Jean-Baptiste, K., Guiziou, S., Chu, J.C., Zemke, J.E. et al.** (2021) A single-cell view of the transcriptome during lateral root initiation in *Arabidopsis thaliana*. *Plant Cell*, **33**, 2197–2220. Available from: <https://doi.org/10.1093/plcell/koab101>
- Garcia-Hernandez, M., Berardini, T., Chen, G., Crist, D., Doyle, A., Huala, E. et al.** (2002) TAIR: a resource for integrated *Arabidopsis* data. *Functional & Integrative Genomics*, **2**, 239–253. Available from: <https://doi.org/10.1007/s10142-002-0077-z>
- Goldbach, H.E. & Wimmer, M.A.** (2007) Boron in plants and animals: is there a role beyond cell-wall structure? *Journal of Plant Nutrition and Soil Science*, **170**, 39–48. Available from: <https://doi.org/10.1002/jpln.200625161>
- Greer, S., Wen, M., Bird, D., Wu, X., Samuels, L., Kunst, L. et al.** (2007) The cytochrome P 450 enzyme CYP96A15 is the midchain alkane hydroxylase responsible for formation of secondary alcohols and ketones in stem cuticular wax of *Arabidopsis*. *Plant Physiology*, **145**, 653–667. Available from: <https://doi.org/10.1104/pp.107.107300>
- Guo, A.Y., Chen, X., Gao, G., Zhang, H., Zhu, Q.H., Liu, X.C. et al.** (2007) PlantTFDB: a comprehensive plant transcription factor database. *Nucleic Acids Research*, **36**, D966–D969. Available from: <https://doi.org/10.1093/nar/gkm841>
- Han, S., Chen, L.S., Jiang, H.X., Smith, B.R., Yang, L.T. & Xie, C.Y.** (2008) Boron deficiency decreases growth and photosynthesis, and increases starch and hexoses in leaves of citrus seedlings. *Journal of Plant Physiology*, **165**, 1331–1341. Available from: <https://doi.org/10.1016/j.jplph.2007.11.002>
- Hedrich, R. & Shabala, S.** (2018) Stomata in a saline world. *Current Opinion in Plant Biology*, **46**, 87–95. Available from: <https://doi.org/10.1016/j.pbi.2018.07.015>
- Horváth, E., Bela, K., Holinka, B., Riyazuddin, R., Gallé, Á., Hajnal, Á. et al.** (2019) The *Arabidopsis* glutathione transferases, AtGSTF8 and AtGSTU19 are involved in the maintenance of root redox homeostasis affecting meristem size and salt stress sensitivity. *Plant Science*, **283**, 366–374. Available from: <https://doi.org/10.1016/j.plantsci.2019.02.005>
- Humphrey, T.V., Bonetta, D.T. & Goring, D.R.** (2007) Sentinels at the wall: cell wall receptors and sensors. *New Phytologist*, **176**, 7–21. Available from: <https://doi.org/10.1111/j.1469-8137.2007.02192.x>
- Javelle, M., Vernoud, V., Rogowsky, P.M. & Ingram, G.C.** (2011) Epidermis: the formation and functions of a fundamental plant tissue. *New Phytologist*, **189**, 17–39. Available from: <https://doi.org/10.1111/j.1469-8137.2010.03514.x>
- Kasajima, I., Ide, Y., Yokota Hirai, M. & Fujiwara, T.** (2010) WRKY6 is involved in the response to boron deficiency in *Arabidopsis thaliana*. *Physiologia Plantarum*, **139**, 80–92. Available from: <https://doi.org/10.1111/j.1399-3054.2010.01349.x>
- Kaya, H., Shibahara, K.I., Taoka, K.I., Iwabuchi, M., Stillman, B. & Araki, T.** (2001) *FASCIATA* genes for chromatin assembly factor-1 in *Arabidopsis* maintain the cellular organization of apical meristems. *Cell*, **104**, 131–142. Available from: [https://doi.org/10.1016/S0092-8674\(01\)00197-0](https://doi.org/10.1016/S0092-8674(01)00197-0)
- Kreplak, J., Madoui, M.-A., Cápal, P., Novák, P., Labadie, K., Aubert, G. et al.** (2019) A reference genome for pea provides insight into legume genome evolution. *Nature Genetics*, **51**, 1411–1422. Available from: <https://doi.org/10.1038/s41588-019-0480-1>
- Lee, S.B., Jung, S.J., Go, Y.S., Kim, H.U., Kim, J.K., Cho, H.J. et al.** (2009) Two *Arabidopsis* 3-ketoacyl CoA synthase genes, *KCS20* and *KCS2/DAISY*, are functionally redundant in cuticular wax and root suberin biosynthesis, but differentially controlled by osmotic stress. *Plant Journal*, **60**, 462–475. Available from: <https://doi.org/10.1111/j.1365-313X.2009.03973.x>
- Li, B., Carey, M. & Workman, J.L.** (2007) The role of chromatin during transcription. *Cell*, **128**, 707–719. Available from: <https://doi.org/10.1016/j.cell.2007.01.015>

- Li, X., Li, Y., Mai, J., Tao, L., Qu, M., Liu, J. et al. (2018) Boron alleviates aluminum toxicity by promoting root alkalinization in transition zone via polar auxin transport. *Plant Physiology*, **177**, 1254–1266. Available from: <https://doi.org/10.1104/pp.18.00188>
- Li, X., Zhang, X., Gao, S., Cui, F., Chen, W., Fan, L. et al. (2022) Single-cell RNA sequencing reveals the landscape of maize root tips and assists in identification of cell type-specific nitrate-response genes. *Crop Journal*, **10**, 1589–1600. Available from: <https://doi.org/10.1016/j.cj.2022.02.004>
- Liang, X., Ma, Z., Ke, Y., Wang, J., Wang, L., Qin, B. et al. (2023) Single-cell transcriptomic analyses reveal cellular and molecular patterns of rubber tree response to early powdery mildew infection. *Plant, Cell & Environment*, **1-16**, 2222–2237. Available from: <https://doi.org/10.1111/pce.14585>
- Liu, H., Hu, D., Du, P., Wang, L., Liang, X., Li, H. et al. (2021) Single-cell RNA-seq describes the transcriptome landscape and identifies critical transcription factors in the leaf blade of the allotetraploid peanut (*Arachis hypogaea* L.). *Plant Biotechnology Journal*, **19**, 2261–2276. Available from: <https://doi.org/10.1111/pbi.13656>
- Liu, Q., Liang, Z., Feng, D., Jiang, S., Wang, Y., Du, Z. et al. (2021) Transcriptional landscape of rice roots at the single-cell resolution. *Molecular Plant*, **14**, 384–394. Available from: <https://doi.org/10.1016/j.molp.2020.12.014>
- Liu, Z., Kong, X., Long, Y., Liu, S., Zhang, H., Jia, J. et al. (2023) Integrated single-nucleus and spatial transcriptomics captures transitional states in soybean nodule maturation. *Nature Plants*, **9**, 515–524. Available from: <https://doi.org/10.1038/s41477-023-01387-z>
- Matthes, M.S., Darnell, Z., Best, N.B., Guthrie, K., Robil, J.M., Amstutz, J. et al. (2022) Defects in meristem maintenance, cell division, and cytokinin signaling are early responses in the boron deficient maize mutant *tassel-less1*. *Physiologia Plantarum*, **174**, e13670. Available from: <https://doi.org/10.1111/ppl.13670>
- McGinnis, C.S., Murrow, L.M. & Gartner, Z.J. (2019) DoubletFinder: doublet detection in single-cell RNA sequencing data using artificial nearest neighbors. *Cell Systems*, **8**, 329–337. Available from: <https://doi.org/10.116/j.cels.2019.03.003>
- Murray, J.A.H., Jones, A., Godin, C. & Traas, J. (2012) Systems analysis of shoot apical meristem growth and development: integrating hormonal and mechanical signaling. *Plant Cell*, **24**, 3907–3919. Available from: <https://doi.org/10.1105/tpc.112.102194>
- O'Neill, M.A., Eberhard, S., Albersheim, P. & Darvill, A.G. (2001) Requirement of borate cross-linking of cell wall rhamnogalacturonan II for *Arabidopsis* growth. *Science*, **294**, 846–849. Available from: <https://doi.org/10.1126/science.1062319>
- O'Neill, M.A., Warrenfeltz, D., Kates, K., Pellerin, P., Doco, T., Darvill, A.G. et al. (1996) Rhamnogalacturonan-II, a pectic polysaccharide in the walls of growing plant cell, forms a dimer that is covalently cross-linked by a borate ester. *Journal of Biological Chemistry*, **271**, 22923–22930. Available from: <https://doi.org/10.1074/jbc.271.37.22923>
- Pommerenig, B., Eggert, K. & Bienert, G.P. (2019) Boron deficiency effects on sugar, ionome, and phytohormone profiles of vascular and non-vascular leaf tissues of common plantain (*Plantago major* L.). *International Journal of Molecular Sciences*, **20**, 3882. Available from: <https://doi.org/10.3390/ijms20163882>
- Poza-Viejo, L., Abreu, I., González-García, M.P., Allauca, P., Bonilla, I., Bolanos, L. et al. (2018) Boron deficiency inhibits root growth by controlling meristem activity under cytokinin regulation. *Plant Science*, **270**, 176–189. Available from: <https://doi.org/10.1016/j.plantsci.2018.02.005>
- Probst, A.V. & Scheid, O.M. (2015) Stress-induced structural changes in plant chromatin. *Current Opinion in Plant Biology*, **27**, 8–16. Available from: <https://doi.org/10.1016/j.pbi.2015.05.011>
- Sakamoto, Y., Kawamura, A., Suzuki, T., Segami, S., Maeshima, M., Polyn, S. et al. (2022) Transcriptional activation of auxin biosynthesis drives developmental reprogramming of differentiated cells. *Plant Cell*, **34**, 4348–4365. Available from: <https://doi.org/10.1093/plcell/koc218>
- Satterlee, J.W., Strable, J. & Scanlon, M.J. (2020) Plant stem-cell organization and differentiation at single-cell resolution. *Proceedings of the National Academy of Sciences of the United States of America*, **117**, 33689–33699. Available from: <https://doi.org/10.1073/pnas.2018788117>
- Schroeder, A., Mueller, O., Stocker, S., Salowsky, R., Leiber, M., Gassmann, M. et al. (2006) The RIN: an RNA integrity number for assigning integrity values to RNA measurements. *BMC Molecular Biology*, **7**, 3. Available from: <https://doi.org/10.1186/1471-2199-7-3>
- Shaw, R., Tian, X. & Xu, J. (2020) Single-cell transcriptome analysis in plants: advances and challenges. *Molecular Plant*, **14**, 115–126. Available from: <https://doi.org/10.1016/j.molp.2020.10.012>
- Shen, W.H. & Xu, L. (2009) Chromatin remodeling in stem cell maintenance in *Arabidopsis thaliana*. *Molecular Plant*, **2**, 600–609. Available from: <https://doi.org/10.1093/mp/ssp022>
- Smykal, P., Aubert, G., Burstin, J., Coyne, C.J., Ellis, N.T.H., Flavell, A.J. et al. (2012) Pea (*Pisum sativum* L.) in the genomic era. *Agronomy*, **2**, 74–115. Available from: <https://doi.org/10.3390/agronomy2020074>
- Sun, X., Feng, D., Liu, M., Qin, R., Li, Y., Lu, Y. et al. (2022) Single-cell transcriptome reveals dominant subgenome expression and transcriptional response to heat stress in Chinese cabbage. *Genome Biology*, **23**, 262. Available from: <https://doi.org/10.1186/s13059-022-02834-4>
- Sun, Z., Jiang, S., Wang, D., Li, L., Liu, B., Ran, Q. et al. (2022) Single-cell RNA-seq of *Lotus japonicus* provide insights into identification and function of root cell types of legume. *Journal of Integrative Plant Biology*, **65**, 1147–1152. Available from: <https://doi.org/10.1111/jipb.13435>
- Szklarczyk, D., Gable, A.L., Lyon, D., Junge, A., Wyder, S., Huerta-Cepas, J. et al. (2018) STRING v11: protein–protein association networks with increased coverage, supporting functional discovery in genome-wide experimental datasets. *Nucleic Acids Research*, **47**, D607–D613. Available from: <https://doi.org/10.1093/nar/gky1131>
- Takahashi, H., Kamakura, H., Sato, Y., Shiono, K., Abiko, T., Tsutsumi, N. et al. (2010) A method for obtaining high quality RNA from paraffin sections of plant tissues by laser microdissection. *Journal of Plant Research*, **123**, 807–813. Available from: <https://doi.org/10.1007/s10265-010-0319-4>
- Tassoni, A., Tedeschi, T., Zurlini, C., Cigognini, I.M., Petrusan, J.-I., Rodriguez, O. et al. (2020) State-of-the-art production chains for peas, beans and chickpeas – valorization of agro-industrial residues and applications of derived extracts. *Molecules*, **25**, 1383. Available from: <https://doi.org/10.3390/molecules25061383>
- Trapnell, C., Cacchiarelli, D., Grimsby, J., Pokharel, P., Li, S., Morse, M. et al. (2014) The dynamics and regulators of cell fate decisions are revealed by pseudotemporal ordering of single cells. *Nature Biotechnology*, **32**, 381–386. Available from: <https://doi.org/10.1038/nbt.2859>
- Voxeur, A. & Fry, S.C. (2014) Glycosylinositol phosphorylcaramides from *Rosa* cell cultures are boron-bridged in the plasma membrane and form complexes with rhamnogalacturonan II. *Plant Journal*, **79**, 139–149. Available from: <https://doi.org/10.1111/tpj.12547>
- Wang, Q., Wu, Y., Peng, A., Cui, J., Zhao, M., Pan, Y. et al. (2022) Single-cell transcriptome atlas reveals developmental trajectories and a novel metabolic pathway of catechin esters in tea leaves. *Plant Biotechnology Journal*, **20**, 2089–2106. Available from: <https://doi.org/10.1111/pbi.13891>
- Wang, Y., Huan, Q., Li, K. & Qian, W. (2021) Single-cell transcriptome atlas of the leaf and root of rice seedlings. *Journal of Genetics and Genomics*, **48**, 881–898. Available from: <https://doi.org/10.1016/j.jgg.2021.06.001>
- Warington, K. (1923) The effect of boron acid and borax on the broad bean and certain other plants. *Annals of Botany*, **37**, 457–466.
- Wei, R., Huang, M., Huang, D., Zhou, J., Pan, X. & Zhang, W.E. (2022) Growth, gas exchange, and boron distribution characteristics in two grape species plants under boron deficiency condition. *Horticulturae*, **8**, 374. Available from: <https://doi.org/10.3390/horticulturae8050374>
- Wimmer, M.A. & Eichert, T. (2013) Review: mechanisms for boron deficiency-mediated changes in plant water relations. *Plant Science*, **203-204**, 25–32. Available from: <https://doi.org/10.1016/j.plantsci.2012.12.012>
- Wong, C.E., Bhalla, P.L., Ottenhoff, H. & Singh, M.B. (2008) Transcriptional profiling of the pea shoot apical meristem reveals processes underlying its function and maintenance. *BMC Plant Biology*, **8**, 73.
- Yang, L.T., Pan, J.F., Hu, N.J., Chen, H.H., Jiang, H.X., Lu, Y.B. et al. (2022) Citrus physiological and molecular response to boron stresses. *Plants*, **11**, 40. Available from: <https://doi.org/10.3390/plants11010040>
- Yang, T., Liu, R., Luo, Y., Hu, S., Wang, D., Wang, C. et al. (2022) Improved pea reference genome and pan-genome highlight genomic features and evolutionary characteristics. *Nature Genetics*, **54**, 1553–1563. Available from: <https://doi.org/10.1038/s41588-022-01172-2>
- Ye, Q., Zhu, F., Sun, F., Wang, T.C., Wu, J., Liu, P. et al. (2022) Differentiation trajectories and biofunctions of symbiotic and un-symbiotic fate cells in root nodules of *Medicago truncatula*. *Molecular Plant*, **15**, 1852–1867. Available from: <https://doi.org/10.1016/j.molp.2022.10.019>

- Yu, M., Shen, R., Xiao, H., Xu, M., Wang, H., Wang, H. et al.** (2009) Boron alleviates aluminum toxicity in pea (*Pisum sativum*). *Plant and Soil*, **314**, 87–98. Available from: <https://doi.org/10.1007/s11104-008-9708-z>
- Zhang, L., He, C., Lai, Y., Wang, Y., Kang, L., Liu, A. et al.** (2023) Asymmetric gene expression and cell-type-specific regulatory networks in the root of bread wheat revealed by single-cell multiomics analysis. *Genome Biology*, **24**, 65. Available from: <https://doi.org/10.1186/s13059-023-02908-x>
- Zhang, T.Q., Chen, Y., Liu, Y., Lin, W.H. & Wang, J.W.** (2021) Single-cell transcriptome atlas and chromatin accessibility landscape reveal differentiation trajectories in the rice root. *Nature Communications*, **12**, 2053. Available from: <https://doi.org/10.1038/s41467-021-22352-4>
- Zhang, T.Q., Chen, Y. & Wang, J.W.** (2021) A single-cell analysis of the *Arabidopsis* vegetative shoot apex. *Developmental Cell*, **56**, 1–19. Available from: <https://doi.org/10.1016/j.devcel.2021.02.021>
- Zhang, T.Q., Lian, H., Zhou, C.M., Xu, L., Jiao, Y. & Wang, J.W.** (2017) A two-step model for de novo activation of *WUSCHEL* during plant shoot regeneration. *Plant Cell*, **29**, 1073–1087. Available from: <https://doi.org/10.1105/tpc.16.00863>